Coordination Chemistry Reviews 255 (2011) 2602–2621

Contents lists available at ScienceDirect

Coordination Chemistry Reviews

journal homepage: www.elsevier.com/locate/ccr

Review

Contributions to the development of ruthenium-based sensitizers for dye-sensitized solar cells

Georgios C. Vougioukalakis[a], Athanassios I. Philippopoulos[b], Thomas Stergiopoulos[a], Polycarpos Falaras[a,*]

[a] Institute of Physical Chemistry, NCSR "Demokritos", Agia Paraskevi, Attiki 15310, Athens, Greece
[b] Laboratory of Inorganic Chemistry, Faculty of Chemistry, School of Sciences, National and Kapodistrian University of Athens, Panepistimiopolis, Zografou 15771, Athens, Greece

Contents

ARTICLE INFO

Article history:
Received 30 August 2010
Accepted 3 November 2010
Available online 12 November 2010

ABSTRACT

The present review article traces the discoveries that were instrumental to the evolution of DSSCs, taking a critical look at the principles of the operation mechanism and insisting on the most important recent developments in the field. We draw our attention mainly to the dye (photosensitizer); the primary processes that take place inside a solar cell, and which are affected by the dye, are also reviewed along

Abbreviations: DSSC, dye-sensitized solar cell; TCO, transparent conductive oxide; VB, valence band; CB, conduction band; V_{max}, maximum voltage; IPCE, incident photon to current conversion efficiency; J_{sc}, short-circuit current; V_{oc}, open circuit potential; *FF*, fill factor; η, overall power conversion efficiency; HTM, hole transporting material; DINHOP, dineohexyl bis-(3,3-dimethyl-butyl)-phosphinic acid; spiro-OMeTAD, 2,2′,7,7′-tetrakis(*NN*-di-p-methoxyphenilamine)-9,9′-spirobifluorene; LUMO, lowest unoccupied molecular orbital; DFT, density functional theory; HOMO, highest occupied molecular orbital; TEMPO, 2,2,6,6-tetramethyl-1-piperidinyloxy; T, 5-mercapto-1-methyltetrazole; CE, counter electrode; PEN, polyethylene naphthalate; TDDFT, time-dependent density functional theory; L, ligand; bpy 2,, 2′-bipyridine; $dcbpyH_2$, 2,2′-bipyridine-4,4′-dicarboxylic acid; MS, mass spectrometry; NMR, nuclear magnetic resonance; FTIR, Fourier-transform infrared spectroscopy; UV–visible, ultraviolet–visible; ESI-MS, electrospray ionization mass spectrometry; MLCT, metal-to-ligand charge transfer; bdmpp, 2,6-bis(3,5-dimethyl-*N*-pyrazolyl)pyridine; CV, cyclic voltammetry; $E_{1/2}$, half-wave potential; bpp, 2,6-bis(1-pyrazolyl)pyridine; Γ, number of adsorbed molecules of the sensitizer adsorbed per square centimeter of geometrical surface area; IMVS, Intensity Modulated Voltage Spectroscopy; IMPS, Intensity Modulated Photocurrent Spectroscopy; L_n, diffusion length.

* Corresponding author. Tel.: +30 210 6503644; fax: +30 210 6511766.
E-mail address: papi@chem.demokritos.gr (P. Falaras).

0010-8545/$ – see front matter
doi:10.1016/j.ccr.2010.11.006

Keywords:
Dye-sensitized solar cells
Dyes
Photosensitizers
Ruthenium
TiO_2

with some of the most significant recent information found in literature that one should keep in mind before designing a novel ruthenium sensitizer. Specific emphasis is given in trying to answer vital questions like defining the optimum number of –COOH anchoring groups and protons that an efficient dye should carry, the correct choice of preparing either a homoleptic or a heteroleptic complex, as well as which counterions are the most suitable. Phenomena such as the role of the adsorption geometry, electrical fields at the double layer, dye-redox couple interaction and recombination effects are also analyzed, in order to show how these factors influence the photoelectrochemical characteristics of the cell. Next, the contributions from our group in the direction of designing, synthesizing, characterizing and evaluating novel ruthenium(II)-based complexes, utilized as photosensitizers in DSSCs, are thoroughly discussed. Two types of Ru(II) complexes are examined: one family mimicking the standard **N719** dye, bearing bidentate ligands, and another, carrying tridendate ligands, resembling the "black dye".

1. Introduction

The increasing demand for energy along with fossil fuels depletion and concerns over global environment preservation render the development of non-polluting renewable power resources an extremely important need [1,2]. Photovoltaic technology is one of the most promising strategies aiming to deal with this problem by harvesting sunlight, thus attaining clean and affordable solar electricity [3,4]. Solid-state photovoltaic cells, based on inorganic semiconductors, have proven to achieve this goal; however, their relatively high production cost and, to a lesser degree, the use of toxic chemicals, imposes limitations on their mass utilization [5,6]. Dye-sensitized solar cells (DSSCs) constitute an appealing alternative to the conventional solid-state cells due to their relatively low production cost, possibility of working indoors and under subdued light conditions, invariant efficiency to the operating temperature, potential transparency and flexibility [7–17]. DSSCs are based on nanocrystalline metal oxide semiconductors sensitized by molecular dyes (photosensitizers) [18,19]. The presence of the dye assures efficient capture of visible light and creation of photoelectrons that are injected directly into the semiconductor; in this case, charge separation is promoted as the electrons and the holes simultaneously reside in different chemical substances (semiconductor and dye, respectively). The above mechanism is totally different in the case of a classical photovoltaic cell; the operation of the latter is based on excitation of electrons from the valence band into the conduction band, while both processes of charge separation and transport take place inside the semiconductor.

The DSSC device (Fig. 1) is basically comprised of two facing electrodes: a transparent photoanode, consisting of a thin nanoparticulate film (7–20 μm) of a mesoporous large band gap semiconductor, modified with a monolayer of dye molecules, which are chemically grafted on the semiconductor's surface via functional groups such as –COOH and $-PO(OH)_2$, and a Pt counter electrode, both deposited on conductive glass substrates. An appropriate medium containing the redox couple (usually I^-/I_3^-) is placed between the two electrodes to transfer the charges.

The photoelectrochemical cycle in DSSCs begins when a dye molecule undergoes transition into its excited state, following absorption of a visible photon (Fig. 2). The photoexcited dye subsequently injects an electron into the conduction band of the semiconductor, i.e. undergoes oxidation; actually, the electron is channeled into the ligand having the lowest π^*-acceptor orbitals and electron injection into the conduction band of the semiconductor takes place from there. Ideally, the photoinjected electron percolates through the nanoparticle network, following a random walk, and gets collected at the back-contact, while the oxidized dye is regenerated to its ground state by taking an electron from the redox couple present in the electrolyte. The collected electrons travel through the external circuit, performing electrical work,

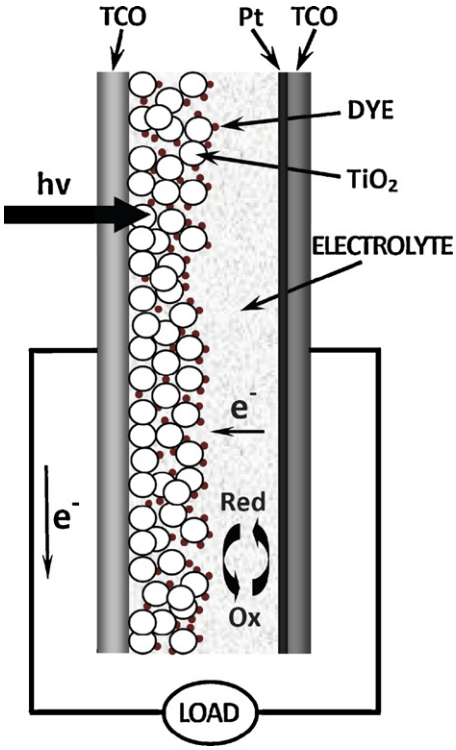

Fig. 1. DSSC operating principles: white circles represent the TiO_2 nanoparticles; brown dots represent the dye molecules; TCO = transparent conductive oxide; red = reducing agent; ox = oxidizing agent.

and eventually reach the counter electrode where they reduce the electron mediator species regenerating the reducing agent and completing the circuit. The device maximum voltage (V_{max}) that can be generated equals the difference between the semiconductor Fermi level and the electron mediator species' (i.e. I^-/I_3^-) redox potential. Overall, the device results in the conversion of photons to electrons, while no chemical species are consumed nor transformed.

To evaluate the performance of a DSSC one has to determine: (i) the incident photon to current conversion efficiency (IPCE), representing the ratio of the collected electrons divided by the incident photons (usually expressed as a function of the excitation wavelength, thus forming the action spectrum); (ii) the short-circuit photocurrent (J_{sc}), which is the photocurrent density per square centimeter obtained when the solar cell is short-circuited; (iii) the open circuit potential (V_{oc}), corresponding to the cell potential when no current flows; (iv) the fill factor (*FF*), defined as the ratio of the maximum electrical power produced by the solar cell divided by the open circuit potential and the short-circuit current; and (v) the overall power conversion efficiency (η), representing

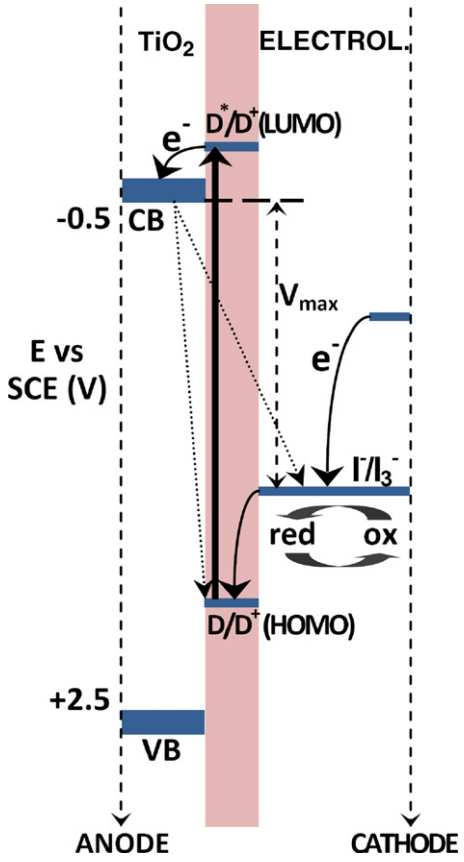

Fig. 2. DSSC energy level diagrams: red = reducing agent; ox = oxidizing agent; $D/D^+/D^*$ = dye in the ground, oxidized, and excited state, respectively; VB = valence band (semiconductor); CB = conduction band (semiconductor); LUMO = lowest unoccupied molecular orbital (dye); HOMO = highest occupied molecular orbital (dye); dotted arrows represent loss mechanisms.

the ratio of the output electrical power of the cell and the flux of the incident light.

Taking into account that cell performance is dictated by the interdependence between the different cell components, in the following sections we briefly summarize the current state of the art concerning each element separately. This will help the reader to better follow the recent developments concerning the "heart" of the device, the dye, which is the main subject of this review article.

1.1. Photoanode

As reported above, the photoanode consists of the semiconductor, deposited on top of a conductive substrate, sensitized by a molecular dye. In the following section, we will draw our attention only to the semiconductor part, since a detailed analysis concerning the dye follows in Sections 1.4 and 2.

The semiconductor plays a very important role in the solar cell, acting as a substrate for dye adsorption and a sink for the transport of the photogenerated electrons. The ideal nanostructured semiconductor should have a mesoporous morphology, giving a high specific surface area along with a network free of recombination sites. Usually, a highly efficient photoelectrode consists of the following structure: first, a compact TiO_2 underlayer is deposited by spray-pyrolysis on the conductive substrate to prevent short-circuits at the back contact/electrolyte interface [20]. Then, a transparent porous film (8–12 μm thick), consisted of interconnected spherical particles in the size range of 15–30 nm, is deposited atop of the first film by screen-printing [21]. Light scattering at long range wavelengths and, consequently, enhanced light harvesting and improved photovoltaic performances are obtained by introducing large TiO_2 particles on top of the active film [22]. Similar effects with the scattering particles could be realized by the use of hollow titania spheres attaining efficiencies as high as 10.3% [23]. Finally, a post-treatment of the composite films with $TiCl_4$, via chemical bath deposition, ensures the creation of a very thin layer of TiO_2 around the particles, increasing electron injection and diminishing recombination with the electrolyte [24]. In order to further optimize charge transport and promote vectorial electron diffusion, more ordered TiO_2 nanostructures have been also employed; these include nanorods [25], wires [26] and tubes [27]. The latter self-assembled nanostructures could be also easily formed on flexible, non-fragile and lightweight substrates, such a Ti metal foil, using electrochemical anodization [28]. In this way, high efficiencies of more than 7.5% could be obtained despite the back-side illumination of the DSSCs [29,30].

1.2. Electrolyte

In DSSCs, the electrolyte regenerates the dye, following electron injection, and is responsible for charge transport between the photoanode and the counter electrode. The most highly efficient DSSCs utilize the iodide/triiodide (I^-/I_3^-) redox couple as electron mediator species, dissolved in an organic electrolyte (e.g. acetonitrile). Due to the fact that these kinds of solvents are volatile, two alternatives have been employed in order to increase the stability in the performance of the DSSC: (i) the use of solvent-free ionic liquid based electrolytes, such as an eutectic melt of 3-alkylimidazolium-based salts, attaining efficiencies of 8.2% [31], and (ii) the application of solid electrolytes with the use of organic polymers and/or inorganic fillers [32] with the highest efficiency attained (7.7%) by a chemically cross-linked polymer gel electrolyte with a dendritic structure [33]. In order to minimize voltage losses, due to the Nernst potential of the iodine-based redox couple, and impede photocurrent leakage due to light absorption by triiodide ions, other redox couples have been also used; these include the Co^{2+}/Co^{3+} (4.2% [34]), TEMPO/$TEMPO^+$ (5.4% [35], where TEMPO is the organic radical 2,2,6,6-tetramethyl-1-piperidinyloxy) and the T_2/T^- (6.4% [36], where T^- represents the 5-mercapto-1-methyltetrazole ion and T_2 stands for its dimer). Finally, a completely solid-state type of cell has been also prepared by substituting the above redox electrolytes with a thin film of an inorganic (e.g. CuI, [37]) or organic semiconductor presenting good *p*-type conductivity. In the latter case, the efficiencies attained using the classical spiro-OMeTAD compound were very promising, reaching values of more than 4.5%.

1.3. Counter electrode

The counter electrode (CE) has the function to transfer electrons arriving from the external circuit to the electrolyte in order to regenerate the redox couple; therefore, an effective CE should primarily possess an excellent catalytic activity for the reduction of triiodide ions. The most commonly used material is platinum, deposited on the conductive substrate by various methods like spin-coating, screen-printing, sputtering, etc. [38]. In order to reduce the cost of the CE and prevent the corrosion of platinum by the iodide solution, other inexpensive, mainly carbonaceous, materials have been also used; these include carbon black (9.1% [39]) and multi-walled carbon nanotubes (7.7%, [40]). Hybrid materials have been also employed, combining polymeric and carbonaceous materials such as polystyrenesulfonate doped poly(3,4-ethylenedioxythiophene) with graphene (4.5% [41]) and polyaniline with carbon black (7.4% [42]). Very recently, a novel counter electrode was fabricated by the electrodeposition of CoS nanoparticles on flexible indium tin oxide/polyethylene naphtha-

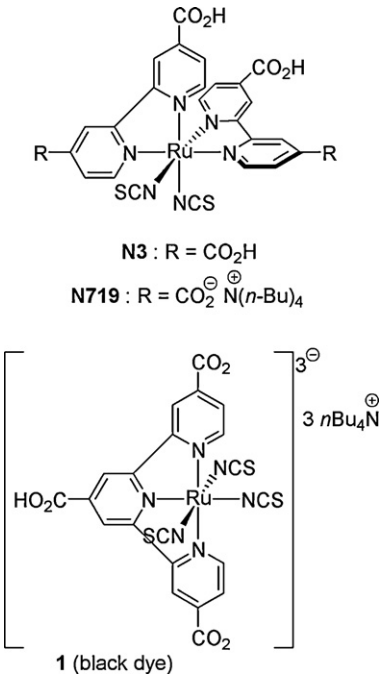

Fig. 3. Molecular structures of ruthenium(II) dyes **N3**, **N719** and black dye (**1**) [45–48].

late (PEN) films, superseding Pt as an efficient electrocatalyst for triiodide reduction [43].

1.4. Sensitizer (dye)

The efficiency of a DSSC largely depends on the charge generation step and, therefore, the sensitizer utilized. Some of the requirements that an efficient sensitizer has to fulfill include [8–15]: (i) a broad and strong absorption, preferably extending from the visible to the near-infrared; (ii) minimal deactivation of its excited state through the emission of light or heat; (iii) a firm, irreversible adsorption (chemisorption) to the semiconductor's surface and a strong electronic coupling between its excited state and the semiconductor conduction band; (iv) chemical stability in the ground as well as in the excited and oxidized states, so that the resulting DSSCs will be stable over many years of exposure to sunlight; (v) a reduction potential sufficiently higher (by ~150–200 mV [44]) than the semiconductor conduction band edge in order to bring about an effective electron injection; and (vi) an oxidation potential sufficiently lower (by ~200–300 mV [44]) than the redox potential of the electron mediator species, so that it can be regenerated rapidly. As expected, another issue concerning dyes is their cost. Ruthenium, for instance, which is currently the most commonly utilized metal in metal-containing dyes for DSSCs, is a rare metal with a relatively high price. Despite the fact that the contribution of the sensitizer to the total cell cost is limited, as efficient light harvesting requires a monolayer of sensitizer molecules, stable long-living ruthenium-based dyes are always highly desirable. Efficient, ruthenium-free sensitizers could also lead to such a cost decrease (vide infra).

A variety of transition-metal complexes and organic dyes has been successfully employed as sensitizers in DSSCs thus far; however, in terms of photovoltaic performance and long-term stability, Ru(II) polypyridyl complexes comprise the most successful family of DSSCs sensitizers. The first high-performance Ru(II) sensitizer was reported in 1993 by Grätzel and co-workers (**N3** and **N719**, Fig. 3) [45,46]. **N3** and **N719**, affording DSSCs with overall power conversion efficiencies of 10.0% and 11.2% respectively, harvest visible light very efficiently with their absorption threshold being at about 800 nm. Equally importantly, both **N3** and **N719**, which essentially differ only in their protonation state, afford a nearly quantitative conversion of incident photons into electric current over a large spectral range. The remarkably improved efficiency of **N719**, when compared to the tetra-protonated parent dye **N3**, was mainly attributed to the increased cell voltage. In 1997, the same research group published the synthesis and evaluation of a terpyridyl analogue of **N3** and **N719**, i.e. "black dye" (**1**, Fig. 3), with a reported overall power conversion efficiency of 10.4% [47,48]. Black dye, a "panchromatic ruthenium(II) sensitizer", sensitizes nanocrystalline TiO_2 cells very efficiently over the whole visible range, extending into the near infrared region up to 920 nm, affording IPCE values that are over 80% over a large spectral range. It is also worth mentioning that the absorption and emission maxima of black dye show a bathochromic shift with decreasing pH, while it exhibits pH-dependent excited state lifetimes. Even though the surface coverage and the extinction coefficient of black dye are lower that the values for **N3**, the spectral response of black dye in the red and near infrared region is enhanced, with respect to **N3**, resulting in higher short circuit photocurrents. Finally, it has to be noted that by raising the haze of TiO_2 electrodes in the near infrared wavelength region, in black dye-sensitized DSSCs, a conversion efficiency of 11.1% may be achieved [49].

Since 1997, a series of modifications of these early Ru(II) complexes have, among others, led to sensitizers with amphiphilic properties and/or extended conjugation, achieving power conversion efficiencies up to 12.3% [50–68]. In 2006, for example, Wu and co-workers reported the synthesis of Ru(II) dye **CYC-B1** depicted in Fig. 4, with the aim of achieving a high absorption coefficient of the main MLCT band [50]. **CYC-B1**, bearing a highly conjugated ligand substituted with alkyl bithiophene groups, was evaluated in DSSCs achieving an overall power conversion efficiency of 8.5%. This power conversion efficiency was 10% higher than that of **N3** (η = 7.7%) under the same cell fabrication and measuring procedures. One year later, the same research group published the synthesis of the structurally related complexes **SJW-E1** and **CYC-B3** (Fig. 4), to further explore the effect of the thiophene moieties [51]. **SJW-E1** and **CYC-B3** afforded DSSCs with conversion efficiencies of 9.0% and 7.4% respectively, whereas **N3** under the same conditions gave η = 8.4%. Also note that the 12.3% efficiency record reported for DSSCs has been reached with Ru(II) sensitizer **Z991**, the mono(tetra butylammonium) salt of **CYC-B1** (vide supra), by using the phosphinate amphiphile DINHOP (dineohexyl bis-(3,3-dimethyl-butyl)-phosphinic acid) as co-adsorbent [57].

Grätzel, Zakeeruddin, Wang, Wu and co-workers have recently developed heteroleptic Ru(II) sensitizers **C101** [53], **C104** [54], **C106** [62], **C107** [64], and **CYC-B11** [59] (Fig. 4) giving DSSCs with power conversion efficiencies of 11.3%, 10.5%, 11.4%, 10.7%, and 11.5% respectively. As shown in Fig. 4, these very successful sensitizers encompass spectator ligands that combine extended π-conjugated systems, seeking to enhance the optical absorptivity of the sensitized TiO_2 films, along with long hydrophobic alkyl chains, aiming at increased tolerance against water attack [69] and, therefore, improved long-term stability. The DSSC devices that utilize the above amphiphilic dyes display extraordinary stability under both thermal stress and exposure with light, making these cells viable for practical, outdoor use applications. In particular, DSSCs sensitized with **C101**, by utilizing either a low volatility 3-methoxypropionitrile electrolyte or a solvent-free ionic liquid electrolyte, showing >9.0% and ~7.4% conversion efficiencies respectively, retain over 95% of their initial performance after 1000 h full sunlight exposure at 60 °C [53]. Likewise, DSSCs using **CYC-B11** and a low-volatility electrolyte (**Z946**) show good performance and stability under prolonged light exposure at 60 °C, albeit with a lower, 7.9% overall conversion efficiency (compared to 11.5%

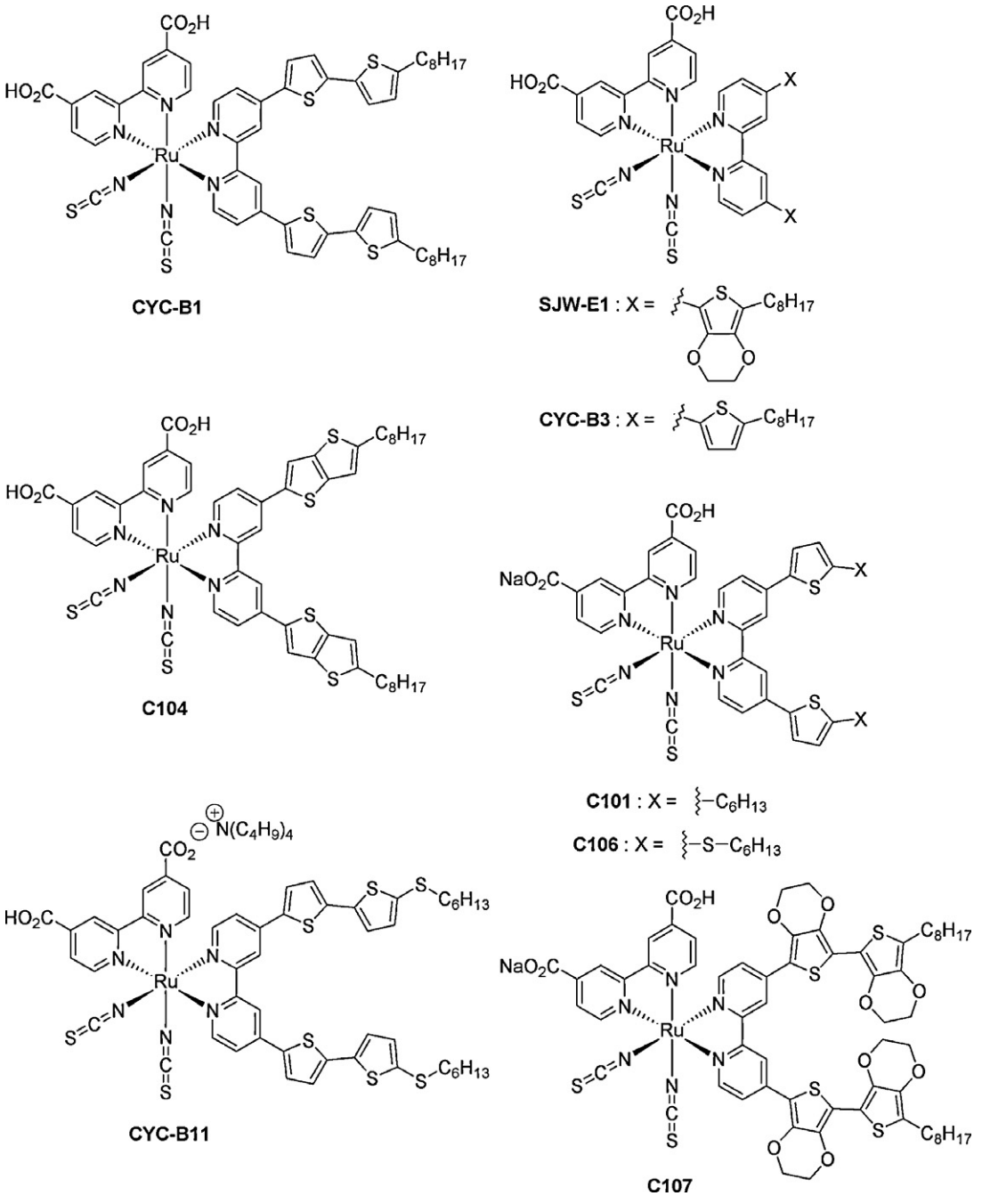

Fig. 4. Molecular structures of heteroleptic ruthenium(II) dyes **CYC-B1**, **CYC-B3**, **CYC-B11**, **SJW-E1**, **C101**, **C104**, **C106** and **C107** [50,51,53,54,59,62,64].

with the volatile acetonitrile-based electrolyte **Z946**) [59]. When a solid state hole transporting material (HTM) was employed instead (spiro-OMeTAD) the corresponding cells, using **CYC-B11**, displayed an efficiency of 4.7%.

In another work, aiming at Ru(II) sensitizers characterized by enhanced molar extinction coefficients, by using ligands with extended π-conjugation, and directionality in the excited state, by appropriately tuning the lowest unoccupied molecular orbital (LUMO) level of the ligand, Nazeeruddin et al. reported the synthesis and photoelectrochemical characterization of dye **N945** shown in Fig. 5 [52]. **N945**-sensitized DSSCs, characterized by a very efficient light harvesting over a large area of the visible spectrum, showed an energy conversion efficiency of 10.8% surpassing **N719**. More recently, Yum et al. published the synthesis of Ru(II) sensitizer **IJ-1** (Fig. 5), a donor-acceptor ruthenium complex bearing a ditolylamine phenyl-ethenyl-2,2′-bipyridine ligand as the secondary electron donor moiety [60]. **IJ-1** sensitizes nanocrystalline TiO_2 cells very efficiently, affording a conversion efficiency of 10.3%. On a different note, Grätzel and co-workers engineered a thiocyanate-free cyclometalated Ru(II) complex (**2**, Fig. 5), which is also a robust panchromatic sensitizer in DSSCs [61]. More specifically, solar cells employing a liquid-based electrolyte and **2** as the sensitizer give overall conversion efficiencies of 10.1%. Density functional theory (DFT) calculations showed that while the highest occupied molecular orbital (HOMO) of **2** is located mostly on ruthenium and the cyclometalated ligand, the LUMO is on the 4-carboxylic acid-4′-carboxylate-2,2′-bipyridine ligand.

Porphyrins, a group of highly conjugated heterocyclic macrocycles, many of which occur in nature, is another class of sensitizers

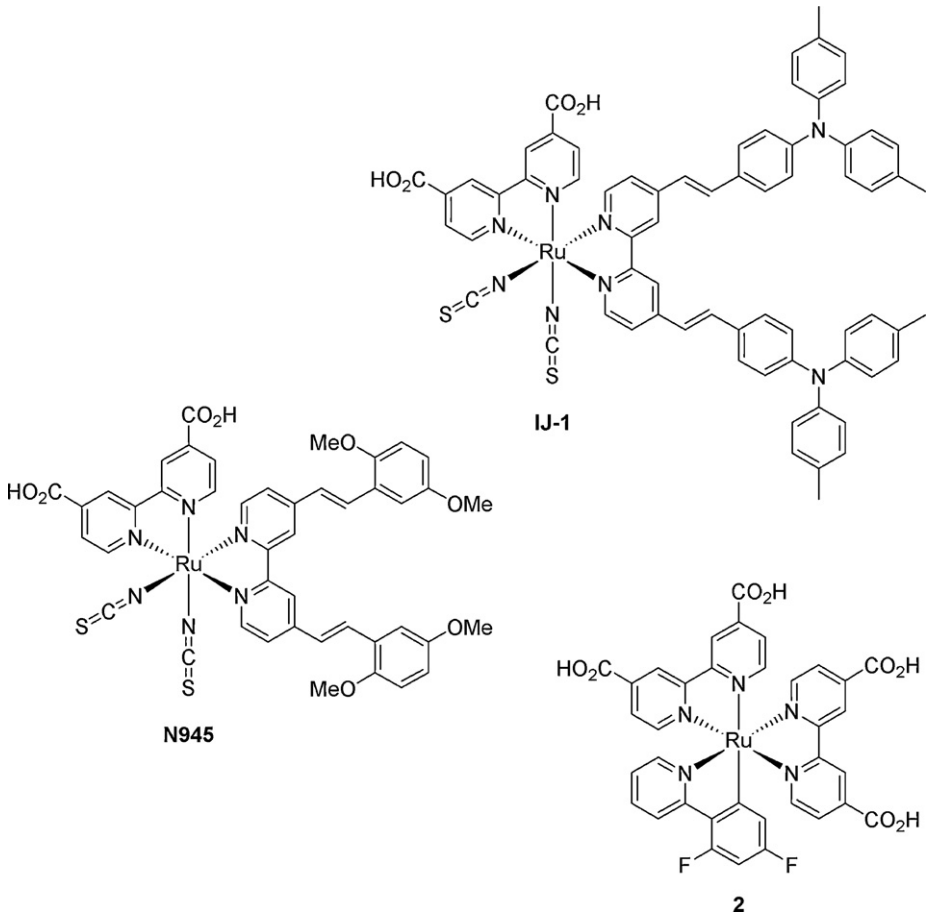

Fig. 5. Molecular structures of ruthenium(II) sensitizers **IJ-1**, **N945** and **2** [52,60,61].

successfully utilized in DSSCs [70–76]. Dye **3** (Fig. 6), the most efficient porphyrin-based sensitizer utilized in DSSCs to date, was reported in 2007 by Officer and co-workers [73]. The four aryl substituents in dark-green **3** act as electron donors, while the malonic acid group as an acceptor. The overall conversion efficiencies of dye **3** in liquid-junction and solid state (using spiro-MeOTAD as HTM) DSSCs were 7.1% and 3.6% respectively. Porphyrins **YD2** [76] and **YD12** [75], shown in Fig. 6, have been more recently synthesized by Yieh, Diau and co-workers. Both **YD2** and **YD12** bear an electron-donating diarylamine moiety with long alkyl chains at a *meso*-position. When used in DSSCs, **YD2** affords a power conversion efficiency of 6.6%. The conversion efficiency of **YD12**, on the other hand, is 6.7% surpassing **N719** (η = 6.1%) under the same cell fabrication and measuring procedures. Besides porphyrins, a variety of other compounds such as phthalocyanines [77–81] and Mg chlorophyls [82,83], as well as Fe [84–86], Cu [87] Os [88,89], Ir [90,91] and Pt sensitizers [92,93] have been also used in DSSCs, though not always very efficiently.

As mentioned earlier, ruthenium-based dyes are rather expensive. This is not only because ruthenium is a rare metal, but also originates from the fact that the purification of the corresponding complexes is generally challenging. As a result, organic dyes, amongst others (vide supra), are lately stimulating intensive research efforts [94–109]. The most important advantages of using organic dyes as sensitizers in DSSCs include their easily tunable physicochemical properties, through suitable molecular design and well established synthetic procedures, along with their ease of purification and high molar absorption coefficients. On the other hand, organic dyes also have weaknesses such as their relatively sharp absorption bands in the visible region, leading to unsatisfactory light harvesting in the entire visible spectrum, along with questionable photostability.

Fig. 7 illustrates four of the most efficient organic dyes used in DSSCs thus far. The synthesis of **TA-St-CA**, for example, was published in 2007 by Park, Kim, and co-workers [96]. Although the dye **TA-St-CA** is based on a very simple donor-π-acceptor molecular design, it affords DSSCs with conversion efficiencies of 9.1% (benchmark **N719** gives 10.1% under the same conditions). Three years later, the same research groups published the synthesis of **TA-DM-CA** [103], by slightly modifying **TA-St-CA** (Fig. 7). The two methoxy groups in **TA-DM-CA** were introduced at the vinylene phenylene moiety in order to both enhance the electron-donating character of the π-conjugated skeleton of the dye and increase its absorption wavelength. DSSCs sensitized with **TA-DM-CA** afford an overall conversion efficiency of 9.7%. Wang and co-workers have also recently published the synthesis and evaluation of dyes **C217** [101] and **C219** [106] shown in Fig. 7. **C217**, employing a lipophilic dihexyloxy-substituted triphenylamine electron donor, a cyanoacrylic electron acceptor, and a binary π-conjugated spacer, yields overall conversion efficiencies of 9.8% and 8.1% in volatile acetonitrile electrolyte and solvent-free ionic liquid electrolyte DSSCs, respectively. Amphiphilic **C219**, the most efficient organic sensitizer utilized in DSSCs thus far, gives an overall conversion efficiency of 10.3% in volatile electrolyte DSSCs. Furthermore, in solvent-free ionic liquid cells, and under a low-light intensity, **C219** affords an efficiency of 8.9%, a characteristic that makes it a potent dye for indoor applications.

Apart from seeking for more efficient dyes, one can also enhance the stability and performance of DSSCs by utilizing surface co-adsorbents [54,78,110–119]. In brief, co-adsorbing the sensitizer

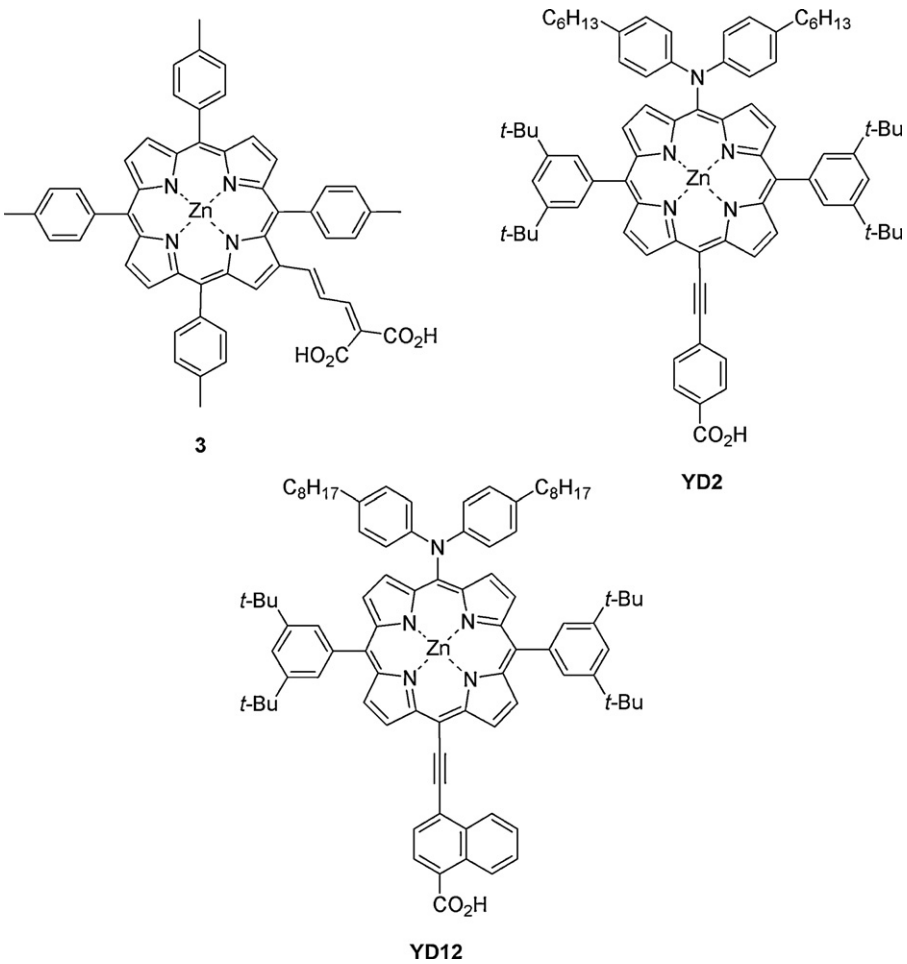

Fig. 6. Porphyrin sensitizers **3**, **YD2** and **YD12** [73,75,76].

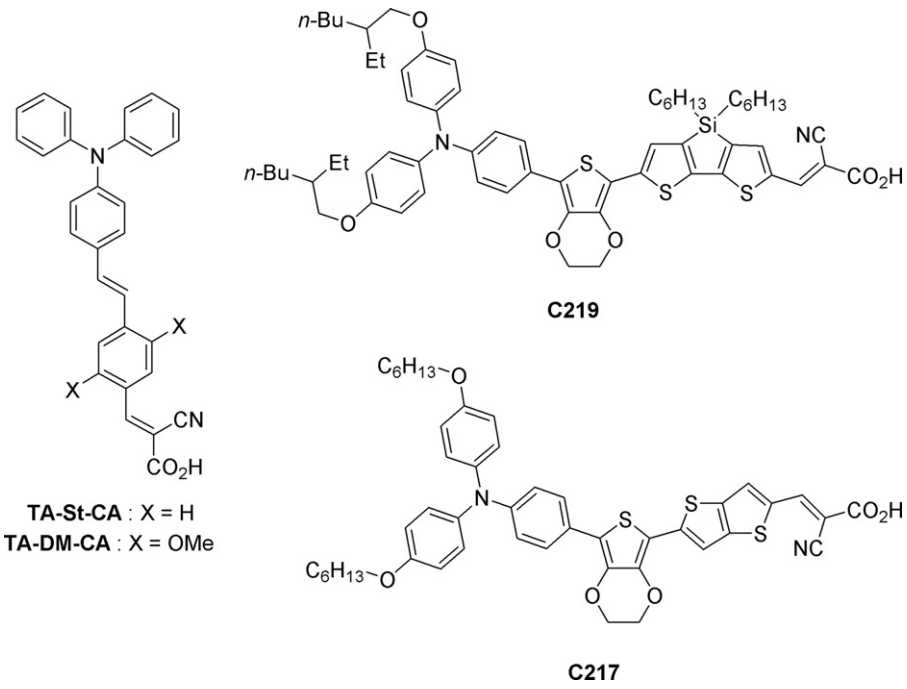

Fig. 7. Organic dyes **TA-St-CA**, **TA-DM-CA**, **C217** and **C219** [96,101,103,106].

with an amphiphilic compound, on the semiconductor, apart from increasing the sensitizer's tolerance against water attack, leads to a more compact dye-amphiphile monolayer than the adsorption of the dye alone would. This "insulating layer" is not only blocking the recombination process, by shielding the corresponding centers, but can also affect the semiconductor's conduction band edge position with respect to the redox energy level of the electrolyte influencing directly the obtained V_{oc}.

2. Dye effects

As discussed above, for an efficient sensitizer some requirements should be fulfilled like tight adsorption on the semiconductor surface, strong absorption of white light, quantitative and quick injection of electrons into the semiconductor conduction band and rapid regeneration by the redox couple. Bearing these issues in mind, scientists have thus far designed and synthesized hundreds of ruthenium complexes. However, throughout all the years, and despite the intensive efforts of the scientific community to optimize the dye, this has not been proven feasible yet (or at least the improvement was not as significant as expected, in relation to champion dyes **N719** and black dye). It is only lately that we managed to concede the complexity of the studied system and recognize the difficulties of designing the perfect dye. Thus, we now acknowledge that the dye does not behave as simply as we have thought of in the beginning and, unfortunately, that many more other key issues have to be controlled in order to achieve the optimum efficiency. In the following, we will draw our attention on all the primary processes taking place inside a solar cell, which are affected by the dye, and we will review some of the most significant and recent information found in the literature that one should keep in mind before setting out to prepare a novel ruthenium complex.

The dye adsorption on the semiconductor surface presupposes that the sensitizer possesses carboxylic (or phosphonate) groups as anchoring moieties. The case of the benchmark **N719** dye needs particular attention and focus, in order to fully understand the effectiveness of a sensitizer in a DSSC. Thus, in this work, several open issues and remaining questions will be considered, following critical review and detailed analysis; e.g.: how many –COOH groups should a good dye have, and how many protons should these groups carry? Should a complex be homoleptic or heteroleptic? Which counterion is the optimum? What is the role of the adsorption geometry? What about dye/redox couple interaction? How all these issues influence the electrical characteristics of the cell (V_{oc} and J_{sc})?

2.1. Adsorption mode

Very recently, a DFT calculation study suggested that the homoleptic **N719** dye (bearing two equivalent bipyridine ligands each functionalized with two carboxylic groups, Fig. 3), adsorbs onto the TiO_2 surface by exploiting three carboxylic groups, leading to high open-circuit potentials when employed in DSSC devices [120]. This turns out to be due to a number of factors, including the increased charge donation from the three anchoring carboxylates to the TiO_2 and, possibly, the formation of a more compact dye layer. Moreover, the adsorption via three anchoring sites should provide additional stability toward dye desorption, a highly desirable requisite for practical DSSC applications and long-term device durability. On the contrary, heteroleptic sensitizers, devised in a way that one of the two bipyridines is specifically functionalized, which necessarily adsorb via carboxylic groups residing on the same bipyridine ligand, give rise to a decrease the open-circuit potential. This is because of the different sensitizer adsorption mode onto TiO_2 compared to homoleptic sensitizers, despite the fact that the chemical functionalization of one bipyridine has little effect on the electronic properties of the second bipyridine [121].

2.2. Dye dipole moment

The sensitizer's dipole moment has a remarkable influence on the open circuit potential and, ultimately, on the efficiency of DSSCs. For instance, dipolar fields of different magnitude and orientation have been found for homoleptic sensitizers (like **N3** or **N719**), which explains their larger open circuit potentials and overall better performance with respect to heteroleptic sensitizers with anchoring groups residing on two different bipyridines [121]. In the latter ones, their adsorption geometry induces a substantial downshift of the TiO_2 conduction band energy, ultimately causing reduced photovoltages [122]. In order to increase V_{oc}, by moving the CB of the semiconductor towards higher energy levels, the dye dipole moment should point outwards from the layer surface [123].

2.3. Number of protons

Another significant parameter in a dye's structure is the number of protons it carries on its molecule; the anchoring groups of the sensitizer that contain protons upon adsorption transfers most of its protons to the TiO_2 surface, charging it positively, in a way that a lot of processes are severely affected [124]. For instance, the surface-bound protons induce a strong localization of unoccupied TiO_2 states in the neighbourhood of the proton positions, these states acting as funnels for the photoexcited electrons. On the other hand, the electric field associated with the surface dipole generated in this fashion enhances the adsorption of the ruthenium complex and assists electron injection from the excited state of the sensitizer into the titania conduction band, favoring higher photocurrents [120]. The strong coupling between dye and TiO_2 computed upon TiO_2 protonation suggests that an adiabatic injection mechanism, in which the same electronic state changes its localization from the dye to the TiO_2 [125] might be responsible for the high rates of electron injection observed experimentally for Ru-polypyridyl dyes on TiO_2. For Ru dyes containing no protons, on the other hand, a nonadiabatic electron injection mechanism, in which the photoexcited electron tunnels from the dye to the TiO_2 conduction band, seems most likely, due to the lack of strong coupling between the dye and TiO_2 [126].

Surface protonation also affects the conduction band edge, in line with the strong open-circuit potential variation observed upon changing the sensitizer's proton content [120]. More specifically, the positive shift of the semiconductor's Fermi level decreases the gap between the redox couple I^-/I_3^- and the Fermi level, resulting in a lower open-circuit potential. If the sensitizer does not carry protons, then the Fermi level moves to more negative values, due to the adsorption of the anionic complex and the cations, thereby leading to a higher value for the open-circuit potential, whereas the value of short circuit current is lowered [127]. Therefore, there should be an optimal degree of protonation for the sensitizer for which the product of short circuit photocurrent and open circuit potential, determining the power conversion efficiency of the cell, is the highest possible [122].

In this context, for a homoleptic dye such as **N719**, a conduction band energy down-shift of as much as 0.1 eV, when varying the number of surface protons from one to two, was experimentally observed [122]. Furthermore, V_{oc} for DSSCs employing heteroleptic sensitizers is significantly lower compared to that observed using homoleptic dyes containing the same number of protons [121]. Then, heteroleptic sensitizers should carry a minimum number of protons in order to obtain the maximum photovoltage.

Moreover, deprotonation of the terminal carboxylic groups causes a different destabilization of the occupied and unoccu-

pied orbitals, which ultimately leads to increased HOMO–LUMO gaps and excitation energies. The fully protonated and fully deprotonated forms of **N719** dye show the smallest and largest, respectively, HOMO–LUMO gap and first excitation energies. This effect is related to the increased electron density on the deprotonated carboxylic groups which raises the energy of the bipyridine π^* orbitals. Therefore, **N719** dye represents an optimal choice with respect to the fully protonated and deprotonated species because of the good compromise between their light-harvesting capability and the alignment of its excited states with the TiO_2 conduction band edge [46].

2.4. The role of counterions

A further reason for the high open-circuit potential delivered by **N719** is related to the choice of the appropriate counterions. Indeed, the bulky tetra butylammonium counterions employed cause a modest (within 0.01–0.03 eV) energy down-shift of the TiO_2 conduction band due to the fact that they stand far away from the semiconductor surface. In contrast, smaller counterions, such as Na^+, which can easily access the surface, lead to a larger conduction band energy down-shift of 0.07 eV [120].

2.5. Electric fields at the TiO_2(dye)/electrolyte interface

Although there are no specific directives concerning the exact way in which the molecular structure of a dye affects its sensitization ability, it is necessary to describe some phenomena that should be kept in mind when proceeding to the design of a new sensitizer. It is generally accepted that the surface electric fields are effectively screened by the large permittivity of TiO_2 and the high ionic strength electrolyte present in the mesopores, at least up to the Helmholtz double layer between the semiconductor and the electrolyte [128]. It was then found that the dye sometimes resides in this region [129]. This fact has two implications: first, the redox potential for a number of sensitizers adsorbed onto TiO_2 follows the changes in band edge potentials of the semiconductor. This means that the standard measurement of the redox potential in solution, using cyclic electrochemical voltammetry, is under question (changes in redox potentials could then lead to variations in injection and regeneration rates) [130]. Second, an electric field (of unique relative orientation) has been found to be created by excited-state injection from one sensitizer molecule, which influences the absorption and photoluminescence spectra of other sensitizer molecules that have not undergone photoinduced electron injection. Although Meyer et al. proposed that this phenomenon will be negligible for efficient dyes such as **N719** [131], the group of Hagfeldt and Boschloo provided a reliable method to quantify the effectiveness of the internal charge transfer of dye molecules under solar cell conditions using electroabsorption spectroscopy [132]. In this way, i.e. if accurate determinations of the samples' absorbance can be made, it is possible to determine correctly the magnitude of the variations in dipole moment normal to the semiconductor surface and, from this, infer the orientation of the dye.

2.6. Influence of the dye on the recombination dynamics at the semiconductor surface

Until now, we have not paid special attention to the fate of the electrons after their injection from the dye into the semiconductor. Although, it was initially accepted that dye molecules block recombination from surface states, decreasing the overall rate and increasing the V_{oc}, some dyes may have an opposite effect as they increase the rate of electron recombination between the photoinjected electrons and the oxidized electrolyte, affecting not only J_{sc} but also decreasing the V_{oc} by hundreds of millivolts [133].

The principal question that arises is what are the "problematic" properties of the dye that catalyze the back-reaction. First, it was confirmed that the recombination dynamics are only weakly dependent upon the dye oxidation potential. In contrast, variation of the spatial separation of the dye cation from the electrode surface resulted in significant variations in recombination dynamics and is indeed an attractive route to modulate these dynamics [134].

The introduction of electron – donating or – withdrawing groups to fine tune the photophysical properties of the dye have occasionally opposite effects. For instance, ruthenium complexes bearing phenanthroline ligands, modified with the introduction of $-NH_2$ or $-NO_2$ groups in order to achieve the desired control over the molecular orbitals (and thus fine tune the molecule's spectroscopic and electrochemical properties), enhanced the electron recombination reaction between the photoinjected electrons at TiO_2 and the oxidized redox electrolyte [135]. Certainly, additional studies are necessary to fully identify the exact molecular structures that lead to poor device performance by increasing back-reaction with triiodides.

Furthermore, some dyes may accelerate recombination by providing a binding site for iodine near the TiO_2 surface [136]. To further investigate the above phemonenon, O'Regan et al. made a modification in the structure of a dye. For instance, a change from an oxygen atom to a sulfur atom in two equivalent positions changed the iodine binding, leaving most other properties relatively unaffected. In this case, a 2-fold increase in the recombination rate and a 20–30 mV loss in V_{oc} was recorded. On this basis, they concluded that it might be more appropriate to add a larger number of weaker donors, instead of one strong. Moreover, within otherwise equivalent dyes, the binding strength correlates with the increase in recombination and, therefore, we should design dyes with the option of a lack of strong binding with iodine [136]. Even the standard dyes (e.g. **N719**) used in DSSCs bind iodine quite strongly without apparently catalyzing recombination. Thus, the mechanism for the acceleration of recombination must involve a combination of the strength of the iodine binding sites, their proximity to the TiO_2 surface, and probably catalysis of the reduction by stabilization of an intermediate [137].

2.7. Dye/redox couple interaction

In general, the interaction between the dye and the electrolyte has not been examined in detail, in terms of dye regeneration or recombination (as described in the previous paragraph). To study this kind of interactions, new and sophisticated state of the art analytical tools are necessary. To this end, Resonance micro-Raman spectrophotoelectrochemistry [138], recently developed in or group [139], has been proved to be a sensitive experimental technique offering high spectral and spatial resolution, able to probe the dye vibrational properties. In addition, interactions of the individual cell components at the corresponding interfaces and most importantly the DSSC response under operating conditions via the application of an external polarization bias can be investigated. More specifically, in situ micro-Raman measurements on DSSCs under real photocurrent conditions has permitted the monitoring of the photoelectrode/electrolyte interface, confirming a strong dependence of the Raman spectra on the applied potential, thereby providing, for the first time, a direct proof of the dye–redox couple interactions [140]. In this direction, detailed investigations by both micro- and macro-Raman spectroscopies on DSSCs, using various polypyridyl-based Ru(II) complexes bearing bidendate or tridendate ligands as well as different functional anchoring groups ($-COOH$, $-PO_3H_2$) have systematically identified the presence of new Raman bands in the low wavenumber region. These bands

are bias dependent and stem from the vibrations of triiodide electrostatically bound to the oxidized form of the dye, providing spectroscopic evidence for the formation of an intermediate complex at the photoelectrode/electrolyte interface. Although these results were supported by elemental theoretical simulations [141] the exact role of this intermediate is not fully understand yet. However, the experimental evidence leads to the conclusion that the formation of the new species does not imply the dye destruction and their presence is sensitive to the effectiveness of each dye used. Intensive research is now in progress to give more insight into this type of interaction.

2.8. Towards the design of the perfect dye

Upon summarizing the above observations, a simple question arises: can we design the perfect dye? De Angelis et al. proposed that if we manage to conjugate the high V_{oc} obtained with the **N719** dye (due to specific adsorption geometry) to the high J_{sc} densities achieved by heteroleptic dyes **Z991** [50] (almost 3 times higher extinction coefficients than that of **N719** [17]), breakthrough DSSC efficiencies exceeding 13% would be obtained [120]. Another idea would be to replace the thiocyanate donor ligands, because, from a chemical stability point of view, this is believed to be the weakest part of the complex. Thus far, however, these efforts have yielded only limited success, because the conversion efficiency achieved with complexes that do not contain NCS^- remain well below 10% [17].

A recent publication from the group of Grätzel, presenting efficient cyclometallated complexes, opens up a new way towards the synthesis of another family of efficient sensitizers [61]. The higher absorbance presented by dye **2** (Fig. 5) compared to that of standard **N719** led to significant photocurrents without sacrificing V_{oc}, attaining overall efficiencies comparable with **N719**. The absorption increase was due to a significant red shift in spectral response, attributed to the fact that the cyclo-metalated ligand is a stronger donor than the two thiocyanate groups, resulting in a destabilization of the Ru(t_{2g}) levels and narrowing the HOMO–LUMO gap of the sensitizer [17].

A very promising alternative, reported more recently, is another thiocyanate-free charge-neutral Ru(II) heteroleptic sensitizer, incorporating a difluoro-phenyl pyridinato ancillary ligand. In this way, a large light-harvesting capability up to 700 nm was obtained leading to a high DSSC performance in conversion efficiency (9.5%, while 8.6% was measured for **N719** under similar conditions) [142]. This improved efficiency arises from two main points: first the presence of thiophene or bithiophene groups enhance the red response of a complex, probably due to lateral π-stacking interactions at the TiO_2 surface [17]; and second, the presence of the fluorine atoms that reduce the Lewis basicity of the pyridyl-pyrazole ligand, possibly by adjusting the Ru(II)/Ru(III) redox potential at a level where rapid regeneration of the sensitizer by the iodide ion is possible, without the need of the sulphur atoms of –NCS pointing towards the electrolyte. Simultaneously, the novel dyes present extremely large potentials (of the order of 810–830 mV). Most probably, this also comes from the presence of fluoride atoms coordinating with Li^+ ions (from the electrolyte), impeding the intercalation into the TiO_2, that normally decreases V_{oc} [143].

To this end, it must be highlighted that with the number of possibilities for dye structures being very large, state of the art theoretical calculations should be employed as a guide for the selection of the most promising candidates for synthesis. For instance, with a new technique recently developed by Jones and Troisi, it is possible to predict the rate of injection of a new chromophore in a few hours using a desktop computer and routine quantum chemistry packages [144]. Similarly, the recently developed scaled opposite-spin configuration interaction singles-doubles code, abbreviated as SOS-CIS(D) [145] appears to offer great accuracy in calculating the UV–visible spectra for novel sensitizers. Finally, a recent study by Pastore et al. has pointed out that a proper time-dependent DFT formulation is capable of providing excitation energies for organic dyes that are of comparable accuracy to the most sophisticated correlated ab initio methods, such as SOS-CIS(D) [146]. In any case, all above mentioned new methods will hopefully assist the experimentalists in the judicious selection of molecular components to engineer the best-performing molecular chromophores for future generation DSSCs [17].

During the last decade, intensive research effort in our group was spent on the preparation of novel ruthenium(II) complexes and their utilization in DSSCs as photosensitizers. We thus have synthesized, characterized and evaluated more than 20 novel ruthenium(II) complexes bearing a series of bi- and tridentate organic ligands. In the following sections, we present an outline of our main contributions in this exciting field and thoroughly refer to the lessons learned from this research activity.

3. Bidentate ruthenium complexes

Two types of Ru(II) complexes with bidentate ligands (L) are discussed below. The first category refers to complexes bearing the classical *cis*-$[Ru(bpy)_2L]^{2+}$ moiety (bpy: 2,2′-bipyridine), while the second to complexes of the formula *cis*-$[Ru(dcbpyH_2)_2L]^{2+}$ ($dcbpyH_2$: 2,2′-bipyridine-4,4′-dicarboxylic acid).

3.1. Synthesis and characterization

3.1.1. Complexes of the general formula cis-$[Ru(bpy)_2)L]^{2+}$

Cationic Ru(II) complexes, of the general formula *cis*-$[Ru(bpy)_2(L^n)]X_2$ [$X = Cl^-$, $n = 1$, L^1 = 4-carboxy-2-(2′-pyridyl) quinoline (complex **4**); $n = 2$, L^2 = 2,2′-pyridine-4,4′-dicarboxylic acid (complex **6**)] and *cis*-$[Ru(bpy)_2(L')_2)]X_2$ [L' = 4-pyridinecarboxylic acid (complex **8**)], were recently reported (Fig. 8) [147]. These dyes were prepared according to a straightforward and reproducible synthetic procedure and physicochemically characterized. Typically, dyes **4**, **6** and **8** were isolated as orange solids by a one-step, high yield procedure, from the direct reaction of *cis*-$[Ru(bpy)_2Cl_2]\cdot 2H_2O$ [148] with the corresponding ligand L in a refluxing $EtOH/H_2O$ mixture (1/1, v/v) or in water. Subsequently, the hexafluorophosphate salts **5**, **7**, and **9** were prepared by the addition of NH_4PF_6 in an aqueous solution of the corresponding chloro derivatives. These salts were obtained as brown solids in moderate yields as air-stable and analytically pure solids. Complexes **4**–**9** were characterized by elemental analyses, mass spectrometry (MS), one- and two-dimensional nuclear magnetic resonance (NMR) spectroscopy experiments, Fourier-transform infrared spectroscopy (FTIR) and Raman spectroscopy, and by ultraviolet–visible (UV–visible) absorption spectroscopy. Repeated attempts to obtain single crystals suitable for X-ray crystallography led to microcrystals or powders of the compounds. Elemental analyses, MS, and NMR data for compounds **4**–**9** are all consistent with the structures shown in Fig. 8.

The FTIR spectra of **4**, **6**, **8** and **5**, **7**, **9** are almost identical in the region of 4000–400 cm^{-1}, apart from the presence of a strong and broad band corresponding to the characteristic stretching mode ν_3(P–F) of the PF_6^- anion. The value of this band is between 831 cm^{-1} to 868 cm^{-1}, while the deformation mode ν_4(P–F) was observed near 557 cm^{-1} [147]. Moreover, in the FTIR spectra of **4**–**9**, the absorption band assigned to the ν(C=O) stretching vibration is present as a broad and medium intensity absorption band ranging from 1709 cm^{-1} to 1735 cm^{-1} (Table 1). It also has to be mentioned that for **4** and **7** (Table 1) the position of the ν(C=O) absorption band

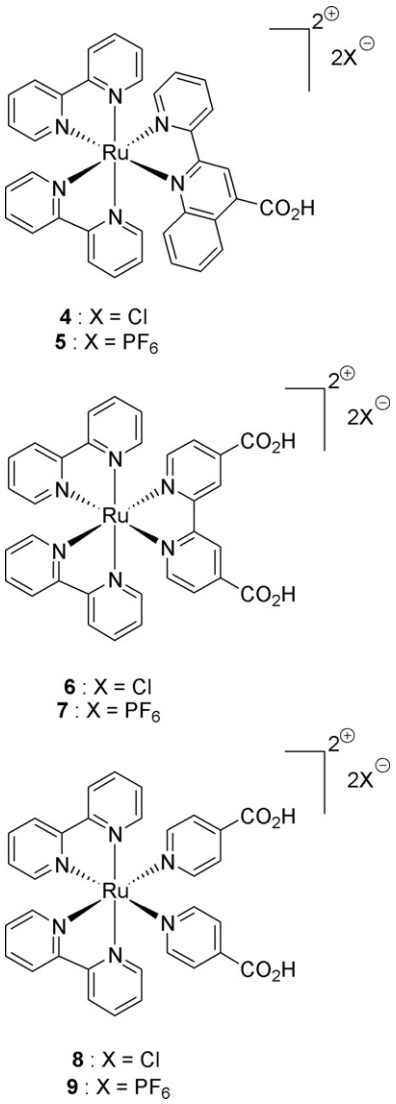

Fig. 8. Molecular structures of sensitizers **4**–**9** [147].

differs significantly from that previously reported in the literature. Additionally, the ν(C=O) stretching vibration upon going from **4** (1735 cm^{-1}) to **6** (1728 cm^{-1}) to **8** (1716 cm^{-1}) appears at lower frequencies, due to the increasing electron density at the Ru(II) metal center. In most of the above complexes, the antisymmetric carboxylate vibration $\nu_{as}(CO_2^-)$ [122] is hard to be observed. For **4** and **6** this vibration is tentatively assigned at 1624 and 1635 cm^{-1} respectively due to overlap with the bpy stretching vibration bands [154] at 1601 and 1602 cm^{-1}.

The Raman spectra of all complexes in the powder form were also recorded giving well-resolved bands, indicating the high purity of these substances. The ν(C=O) stretching vibration of **6** and **7**, present as a medium intensity absorption band at 1728 cm^{-1} and 1709 cm^{-1} respectively, was not detected in the other four complexes described. The Raman spectra of the TiO_2 photo-electrodes sensitized with complexes **6** and **7** present significant changes, compared to the spectra of the pure solids, such as broadening and frequency shift of the ring stretching modes at 1480, 1545, and 1605 cm^{-1}, which is characteristic of the dye chemisorptions to the titania surface [140,155]. On the other hand, the Raman spectra of TiO_2-grafted complexes **4**, **8** and **9** are dominated by the anatase TiO_2 bands; thus, the contribution of the dyes to these spectra is relatively weak. The molecular composition of compounds **4**–**5**, **6**–**7**, and **8**–**9** was further confirmed by electrospray ionization mass spectrometry (ESI-MS). For complexes **5**, **6** and **7** the molecular ion peaks $[M/2]^{2+}$ were detected at m/z = 332 (**5**) and m/z = 329 (**6** and **7**) in the corresponding positive mode ESI-MS spectra.

The absorption spectra of complexes **4**–**5** and **6**–**7** in ethanol (10^{-5} M), display a metal-to-ligand charge transfer (MLCT) transition band in the 452 to 454 nm region [156] with molar extinction coefficients (1.3×10^4 M^{-1} cm^{-1} to 1.7×10^4 M^{-1} cm^{-1}) comparable or even higher than that of **N719** (1.4×10^4 M^{-1}). However, the visible spectra of **8**–**9** is dominated by two distinct and broad transitions at 459 and 354 nm for **8** and 458 and 351 nm for **9**. Furthermore, upon going from **4** and **5** to **8** and **9**, λ_{max} is slightly shifted toward the red, denoting that, as expected, the absorbance of the complexes depends on the nature of the carboxyl-bearing ligand. Interestingly, the hexafluorophospate analogues **5**, **7** and **9** present higher extinction coefficients in the MLCT absorption bands, suggesting that they can act as much more efficient light harvesting molecular antennae (vide infra).

The absorbance spectra of the TiO_2 films sensitized by dyes **7**–**9**, revealed broad absorption band of rather low intensity. The corresponding absorption spectra of dyes **4**–**6** is dominated by strong and quite broad absorption bands in the visible centered at about 460 nm. Upon grafting onto the titania surface, the absorption band of dyes **5**, **6** and particularly **7** is clearly red-shifted in contrast to the blue shift observed in other reported dyes [157]. This shift to higher wavelengths was attributed to the electronic coupling between the adsorbed dyes and TiO_2 [158]. Note that the red shift of the dye absorption in the visible favors solar light harvesting. In this respect, it was verified that the absorption efficiency of the dyes also depended on the concentration of the dye adsorbed on the TiO_2 film. Dyes **4**, **8** and **9** were less efficiently adsorbed than **5** and **6**–**7**. In fact, the amount of adsorbed dye on a TiO_2 film was determined by desorbing the dye from the TiO_2 surface into a 0.01 M NaOH aque-

Table 1
ν(C=O) absorption bands (cm^{-1}) of *cis*-$[Ru(bpy)_2)L]^{2+}$ complexes **4**–**9**.

Complexes[a]	ν(C=O)[b] (cm^{-1})	$\nu_s(CO_2^-)$[b] (cm^{-1})	ν(C–O)[b] (cm^{-1})	Reference
cis-$[Ru(bpy)_2(L^1)]Cl_2$ (**4**)	1735	1380	1211	[147]
cis-$[Ru(bpy)_2(L^1)]Cl_2$	1610	–	–	[149,150]
cis-$[Ru(bpy)_2(L^1)](NO_3)_2$	1607	–	–	[149,150]
cis-$[Ru(bpy)_2(L^1)](PF_6)_2$ (**6**)	1714	1395?	1222	[147]
cis-$[Ru(bpy)_2(L^2)]Cl_2$ (**5**)	1728	1397	1221	[147]
cis-$[Ru(bpy)_2(L^2)](PF_6)_2$ (**7**)	1709	1366	1230	[147]
cis-$[(Ru(bpy)_2(L^2)](PF_6)_2 \cdot 1.5H_2O$	1736	–	–	[151,152]
cis-$[Ru(bpy)_2(L^2)](PF_6)_2$	1716	–	–	[151,152]
cis-$[Ru(bpy)_2(L^2)](PF_6)_2$	1734	–	–	[153]
cis-$[Ru(bpy)_2(L')_2]X_2$ (**8**)	1716	–	1228	[147]
cis-$[Ru(bpy)_2(L')_2](PF_6)_2$ (**9**)	1715	–	–	[147]

[a] bpy: 2,2′-bipyridine.
[b] Band positions of the specified molecular vibrations in the corresponding vibrational spectra.

ous solution. Typical dye uptakes were 3.4×10^{-7} mol cm^{-2} (**4**), 2.2×10^{-7} mol cm^{-2} (**5**), 2.3×10^{-7} mol cm^{-2} (**6**) and 2.4×10^{-7} mol cm^{-2} (**7**). Notably, these values are larger than that of commercial **N719** (1.5×10^{-7} mol cm^{-2}), which was also used as a reference. For dyes **8** and **9**, the titania film after impregnation into a 0.3 mM ethanol solution of the dye, afforded a very faint color implying that the amount of the dye adsorbed was negligible, which is in accord with the Raman spectrum of these compounds upon grafting to the TiO_2 films.

3.1.2. Complexes of the formula *cis*-[Ru(dcbpyH$_2$)$_2$L]$^{2+}$

As a continuation of the above reported class of compounds we have more recently focused on the corresponding *cis*-[Ru(dcbpyH$_2$)$_2$L]$^{2+}$ complexes [159]. The latter were prepared from *cis*-[Ru(dcbpyH$_2$)$_2$Cl$_2$] after removal of the halide ligands with $AgNO_3$ and subsequent addition of a stoichiometric amount of the corresponding ligand L (L^1 = 4-carboxy-2-(2′-pyridyl)quinoline, L^4 = 2-(2′-pyridyl)quinoxaline). Thus, the cationic complexes of the formulae *cis*-[Ru(dcbpyH$_2$)$_2$(L^4)](NO$_3$)$_2$ and *cis*-[Ru(dcbpyH$_2$)$_2$(L^1)](NO$_3$)$_2$ (**10** and **11** respectively, Fig. 9) were isolated in a pure form as red-brown microcrystalline solids, after repeated crystallizations of the mother liquor. The homoleptic complex [Ru(dcbpyH$_2$)$_3$]Cl$_2$ was also isolated as a side product from both reactions. The new sensitizers were fully characterized in terms of their spectroscopical, optical and electrochemical properties. In the FTIR spectra of **10** and **11**, the ν(C=O) stretching vibration appears at 1719 and 1718 cm^{-1} respectively, while the antisymmetric stretching mode (ν_3) of the nitrate ion is present as a very strong and intense broad band at 1385 cm^{-1}.

The absorption spectra of complexes **10**–**11** and of the **N719** dye were recorded in MeOH (10^{-5} M). Complex **10** displays an intense and composite band in the visible region at 491 and 448 nm ($\varepsilon = 1.1 \times 10^4$ and 1.4×10^4 M^{-1} cm^{-1}), attributed to the metal-to-ligand charge transfer transition bands (MLCT). On the other hand, the visible spectrum of **11** shows a broad band at 466 nm with a molar absorption coefficient of 1.6×10^4 M^{-1} cm^{-1}. Two distinct shoulders at 369 and 351 nm and an absorption band at 307 nm are assigned to intraligand π–π^* charge-transfer transitions localized on the dcbpyH$_2$ and the L^1 ligands. From **10** to **11** there is a characteristic hypsochromic shift (25 nm, 0.13 eV, 1100 cm^{-1}), attributed to the presence of the electron-withdrawing –COOH group on the coordination sphere of the incoming 4-carboxy-2-(2′-pyridyl)quinoline ligand, as opposed to the nitrogen atom contained in the 2-(2′-pyridyl)quinoxaline ligand [160]. Finally, detailed analysis showed that both dyes present no emission at ambient temperature in methanol solutions. The same result was also confirmed with degassed solvents.

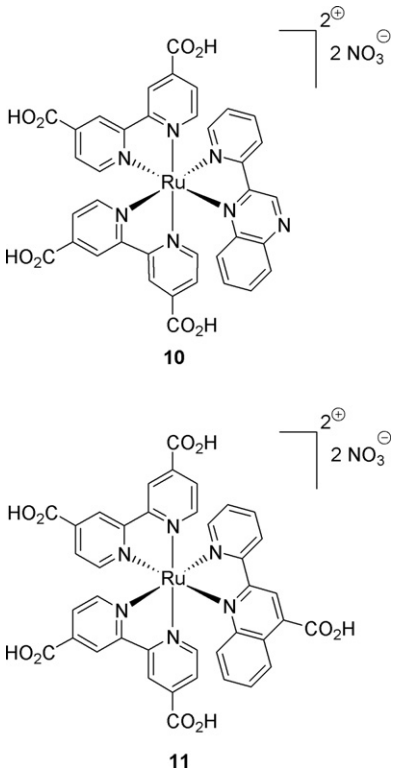

Fig. 9. Molecular structures of ruthenium(II) dyes **10** and **11** [159].

3.2. Photoelectrochemical studies

The above described Ru(II) complexes were used to sensitize TiO_2 photoelectrodes of optimum structure; then, sandwich-type DSSCs were assembled using a PMII-ionic liquid based electrolyte (purchased from Dyesol) and illuminated by a solar simulator providing a power density of 100 mW cm^{-2} (1 sun, AM 1.5). The cell parameters, including the overall photovoltaic efficiency, are summarized in Table 2. The two newly synthesized dyes (**4** and **5**) attained extremely poor efficiencies of the order of 0.01–0.03%, probably due to the single carboxyl group attached on the modified quinoline ligand, obstructing a strong bonding on the semiconductor's surface and thus a good electronic coupling with the density of states in TiO_2 [157]. On the other hand, dyes bearing two (non-chelating) isonicotinic acids as ligands, i.e. carrying two carboxyl groups (instead of one), did not improve much the efficiencies; dye **8** gave only 0.01% while the dye having PF_6^- as the counter ion (**9**) attained a higher efficiency of 0.4%, attributed to the bet-

Table 2
Electronic spectroscopic data of dyes bearing bidendate ligands and performance parameters of TiO_2-based DSSCs sensitized by the same dyes.

Ru-photosensitizer	ε[a] (10^4 dm^3 mol^{-1} cm^{-1}) (λ_{max}[b] (nm))	J_{sc}[c] (mA cm^{-2})	V_{oc}[d] (mV)	*FF*[e]	η[f] (%)
4	1.3 (452)	0.08	391	0.48	0.01
5	1.3 (454)	0.12	432	0.54	0.03
6	1.3 (454)	3.89	585	0.55	1.3
7	1.7 (454)	3.07	571	0.58	1.0
8	0.7 (354), 0.5 (459)	0.06	258	0.38	0.01
9	1.7 (351), 1.0 (458)	1.04	559	0.59	0.4
10	1.4 (448), 1.1 (491)	0.38	390	0.59	0.1
11	1.6 (466)	4.00	569	0.69	1.6
N719	1.4 (383), 1.4 (527)	15.11	755	0.64	7.3

[a] Molar absorption coefficient.
[b] Wavelength of maximum absorption.
[c] Short-circuit current.
[d] Open circuit potential.
[e] Fill factor.
[f] Overall power conversion efficiency.

ter stabilization of the complex due to the greater size of PF_6^- (in comparison with the small chloro anion).

However, sensitizers bearing a dicarboxy-bipirydine ligand gave higher efficiencies, attaining η values over 1.0%; especially dye **7** attained an efficiency of 1.3% with a short circuit photocurrent density (J_{sc}) of 3.89 mA cm^{-2}, an open circuit potential (V_{oc}) of 585 mV and a fill factor (*FF*) of 0.55. Under similar experimental conditions, dye **7** gave 1.0%. As seen in the previous section, the absorbance of these two dyes was higher (broader spectrum in combination with a higher absorption coefficient [147]) than that found for the other dyes (**4**, **5**, **8** and **9**), implying a stronger adsorption of these complexes on TiO_2 due to the chelating nature of the bipyridine ligand carrying two protons. The molecular structure of these complexes also favored their energetic position, as the interface energy diagrams have previously shown that the excited states of dyes **6** and **7** match well the lower bound of the semiconductor conduction band, thus minimizing energy losses during the electron transfer process [147]. This better matching plays a crucial role, making electron injection to TiO_2 more favorable.

Certainly, the two optimum dyes present significantly lower efficiencies than those gained by the standard **N719** dye (η = 7.3%, Table 2), despite their similarity in molecular structure, probably due to the absence of the thiocyanate (–NCS) ligands, which stabilize the t_{2g} molecular orbitals, lowering the dye energy levels and causing an important red shift to the corresponding MLCT absorption bands. Studies are in progress with the aim of further improving the sensitizing properties of the dye-sensitized solar cells based on the aforementioned dyes containing the *cis*-$[Ru(bpy)_2]^{2+}$ core.

Two other Ru(II) complexes (**10** and **11**) bearing the modified quinoline ligand in conjunction with two bicarboxy-bipirydine ligands (complex **11** bears a carboxy-(pyridyl)quinoline ligand) were also prepared and used for the fabrication of DSSCs. Despite the fact that the dye uptake was similar for the two new complexes, being analogous to the coverage measured for **N719** dye (these results will be published in due course), the short circuit photocurrent density (less than 0.5 mA cm^{-2}) of complex **10** was significantly lower (about ten times) than the J_{sc} of dye **11** (4 mA cm^{-2}), probably due to the formation of dye agglomerates that cannot contribute to sufficient electron injection to the conduction band of the semiconductor. Accordingly, the overall efficiency of complex **10** was very low (η = 0.1%), while in the case of complex **11** an overall energy conversion efficiency of 1.6% was obtained. Furthermore, the V_{oc} of the **11**-cell (being 569 mV) was more than 200 mV larger than that of the dye **10** (V_{oc} = 390 mV), implying less recombination or a positive shift of the conduction band edge of the TiO_2 caused by the protons that dissociate from the carboxyl groups of the ruthenium dyes grafted on titania [157]. This is in accordance to previously reported studies for Ru(II) phenanothroline complexes [161] and for the *cis*-$[Ru(bpy)_2(L^2)]^{2+}$, *cis*-$[Ru(bpy)_2(dcbpyH_2)]^{2+}$ [147] and Ru(bpp)(dcbpyH)(X)] complexes (bpp = 2,6-bis(*N*-pyrazolyl)pyridine, X = Cl^-, NCS^-) [162] prepared by our group (vide infra). Furthermore, a comparison of the power conversion efficiency of the best dye **11** (η = 1.6%) with that for *cis*-$[Ru(bpy)_2(L^2)]^{2+}$ (η = 0.03%) [147] reveals the importance of the $dcbpyH_2$ anchoring group on the performance of the corresponding DSSC.

4. Tridentate ruthenium complexes

4.1. Synthesis and characterization

The synthesis of bipyrazolyl(pyridine)-coordinated Ru(II) dyes **12** [163] and **13** [164], shown in Fig. 10, was published in 2002. **12** was prepared in moderate yield by consecutively reacting $RuCl_3 \cdot 3H_2O$ with 2,6-bis(3,5-dimethyl-*N*-pyrazolyl)pyridine (bdmpp), $dcbpyH_2$ in the presence of LiCl and triethylamine, and NH_4PF_6 (to exchange Cl^- for PF_6^-) [163,164]. **13** was then prepared in excellent yield by reacting **12** with NaNCS [164].

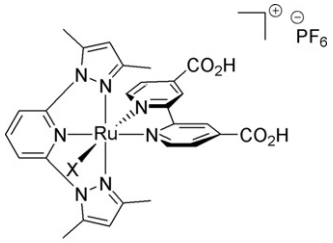

12 : X = Cl
13 : X = NCS

Fig. 10. Bipyrazolyl(pyridine)-bipyridine Ru(II) sensitizers **12** and **13** [163,164].

Cationic complexes **12** and **13** were fully characterized by electrospray ionization mass spectrometry (ESI-MS), one- and two-dimensional NMR spectroscopy experiments, FTIR spectroscopy, cyclic voltammetry (CV), and UV–visible absorption spectroscopy. In the FTIR spectra of **12**, the absorption band at 1715 cm^{-1} corresponds to the carboxylate C=O bond stretching, while the bands between 1231 cm^{-1} and 1262 cm^{-1} originate from the C–O bond stretching. The related bonds in the FTIR spectra of **13** resonate at 1713 cm^{-1} and between 1232 cm^{-1} and 1262 cm^{-1}. Moreover, the strong absorption band at 2109 cm^{-1} was assigned to the *N*-bonded NCS ligand [ν(C=N) stretching vibration] and a band at 771 cm^{-1} to the ν(C=S) stretching vibration. The molecular ion peaks (M^+) of complexes **12** and **13** were detected at m/z = 648 and m/z = 671.2, in the corresponding ESI-MS spectra (positive mode), along with several expected fragments. The structures depicted in Fig. 10 are also fully consistent with the obtained NMR data (i.e. chemical shifts, integrations, peak multiplicity, and 2D homo- and hetero-nuclear coupling experiments). Additionally, both dyes show well-defined reversible oxidation-reduction waves attributed to the Ru(II)/Ru(III) redox couple. The oxidation-reduction processes for complexes **12** and **13** were observed at half-wave potentials ($E_{1/2}$) of + 0.81 V and + 0.795 V versus Ag/AgCl, respectively. A peak observed at −0.612 V in the voltammogram of **13** was attributed to the first ligand-centered reduction.

The electronic spectra of complexes **12** and **13** in solution (MeOH, 10^{-4} M), which are typical of Ru(II) diimine systems, present a quasi-similar behavior with three absorption maxima of very high intensity (ε > 20,000 M^{-1} cm^{-1}) in the visible, attributed to metal-to-ligand charge transfer (MLCT) processes from a d-orbital of the metal to a π^*-orbital of a ligand. Both dyes show an absorption hump at about 570 nm, while their absorption coefficients are still high ($\varepsilon \sim 3000$ M^{-1} cm^{-1}) even at 650 nm. Thus, both **12** and **13** absorb over the most of the visible, but also expand with a tail in the near-IR region. The spectra of both dyes are blue-shifted compared with that of **N3**, although they present significantly higher absorbance extinction coefficients. These dissimilarities verify that the bdmpp ligand is involved in the MLCT transitions and that this ligand is a weaker acceptor than dcbpy. Furthermore, halide ions are stronger σ- and π-donors than the NCS ligand and someone would expect a blue shift in the absorbance spectra of **13** in comparison with **12**; however, a slight red-shift (~10 nm, 0.07 eV or 570 cm^{-1}) was observed, which was attributed to π-back donation from the Ru(II) center to the isothiocyanato ligand.

The absorbance spectra of the dye-sensitized TiO_2 films, by both **12** and **13**, reveal a strong and broad absorption in the visible centered at 463 nm [162]. The spectra for the two sensitized photoelectrodes are almost identical and cover a good part in the visible region, although the spectrum of the film sensitized by **13** expands

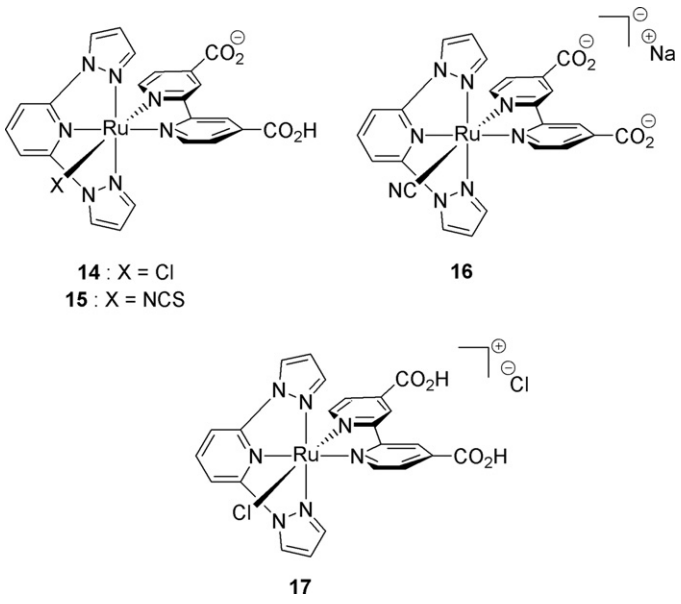

Fig. 11. Bipyrazolyl(pyridine)-bipyridine Ru(II) dyes **14**–**17** [165].

with a somewhat longer tail up to about 730 nm. This small change in the tail of the absorption spectrum shows that the low energy MLCT transition is only slightly influenced by the presence of a π^* low-lying orbitals ligand like NCS. The fact that this change is not observed in solution most probably originates from the dependence of the spectra on the solvent (MeOH); in other words, a possible exchange of the anionic ligand with a neutral solvent molecule may slightly shift a MLCT band. Also, the absorbance spectra of the modified TiO_2 thin film photoelectrodes are broader than the corresponding spectra of the dyes in MeOH suggesting an important change in the energy levels of HOMO and LUMO of the complexes. This was rationalized on the basis of a strong interaction between the dye molecules and the TiO_2 substrate, and was considered as a confirmation of the chemical binding of the sensitizers to the semiconductor's surface via the formation of ester-like linkages.

Heteroleptic Ru(II)-based complexes **14**–**17** (Fig. 11) have been also synthesized, spectroscopically characterized, and evaluated in DSSCs [165]. **14** was prepared almost quantitatively by reacting $Ru(bpp)Cl_3$ (bpp = 2,6-bis(1-pyrazolyl)pyridine) [166] with $dcbpyH_2$ in the presence of triethylamine (acting as both reducing and deprotonating agent). Halide substitution reactions of **14** with either NCS (NH_4NCS) or CN (NaCN) led to the neutral and anionic sensitizers **15** and **16** in 89% and 67% isolated yield, respectively. Also, the reaction of **14** with HCl quantitatively afforded the cationic Ru(II) complex **17**. Complexes **14**–**17** (Fig. 11) have been obtained analytically pure by simple crystallizations, that is, without the need for use of time-consuming chromatographic purification, and are all air stable in the solid form. **14**–**17** were characterized by elemental analysis, mass spectrometry, one- and two-dimensional NMR spectroscopy experiments, FTIR spectroscopy, cyclic voltammetry, as well as by UV–visible absorption and emission spectroscopy.

Elemental analyses, mass spectrometry, and NMR data for compounds **14**–**17** are consistent with the structures shown in Fig. 11. Note, that care should be taken when dissolving **14** in $(CD_3)_2SO$, as it undergoes slow chloride substitution by solvent molecules. FTIR spectra of complexes **14** and **15** are almost identical, as expected for isostructural compounds, except for the presence of a strong NCS band at 2109 cm^{-1}, in complex **15**, assigned to *N*-bonded NCS ligand [ν(C=N) stretching vibration]. The presence of a less intense band at 815 cm^{-1} was assigned to the ν(C=S) stretching vibration. Also, the characteristic ν(C=N) stretching vibration Raman band in **15** appears at 2112 cm^{-1}, slightly shifted compared to the value observed by IR. Both **14** and **15** exhibit a broad and medium intensity IR absorption band at about 1718 cm^{-1}, assigned to the ν(C=O) stretching vibration. This band has a slightly higher frequency than that of **12** and **13** (Fig. 10), an observation that was attributed to the higher electron density at the Ru(II) center of complexes **12** and **13** bearing the methyl-substituted pyrazolyl-pyridine ligand bdmpp. Anionic complex **16**, on the other hand, shows no IR bands above 1700 cm^{-1}, confirming the absence of protonated carboxylic groups. Instead, there is a very strong and broad band at 1600 cm^{-1}, assigned to the $\nu(CO_2^-)$ antisymmetric stretching vibration. Furthermore, the strong band at 1377 cm^{-1} was assigned to the symmetric vibration mode of the carboxylate group [$\nu(CO_2^-)$]. The presence of the terminal cyanido ligand in **16** is confirmed by a medium intensity absorption band at 2077 cm^{-1}, in accordance with similar ruthenium complexes from the literature. The Raman spectrum of complex **16** showed very well resolved bands, which are indicative of the high purity of this compound, with the characteristic ν(CN) mode as a medium intensity band at 2076 cm^{-1}. Finally, cationic **17** displays the ν(C=O) stretching vibration at 1718 cm^{-1} and the ν(C–O) mode at 1230 cm^{-1} as a medium intensity band, while the Raman spectrum of **17** reveals a medium intensity band for the ν(Ru–Cl) stretching mode at 335 cm^{-1}, in line with literature precedence.

Well-defined reversible oxidation-reduction waves, attributed to the Ru(II)/Ru(III) redox couple, were obtained for dyes **14** and **17**. The neutral dye (**14**) has a lower oxidation potential (+ 0.68 V versus Ag/AgCl) than cationic **17** (+0.73 V versus Ag/AgCl). Taking into account that the onset of the dye absorption spectra is the same, electron injection is expected to be more efficient for **17** compared to **14** (vide infra).

The solid-state structures of complexes **12** (Fig. 10) and **16** (Fig. 11) have been also determined by single crystal X-ray diffraction [165]. Both complexes reveal distorted octahedral geometry around the Ru(II) metal ion. The ligands bdmpp and bpp chelate meridionally via their three nitrogen atoms, forming a plane with one of the nitrogens of the $dcbpyH_2$ ligand. The second nitrogen atom of $dcbpyH_2$ and the chloride ligand occupy the axial positions. Distortion results from the constrained bite angle of the chelating tridentate bipyrazolyl(pyridine) of 156.5(3)° and 156.15(3)° respectively. Because of this constrained bite angle, the ruthenium-nitrogen bond to the pyridine nitrogen (of the bipyrazolyl ligands) is shorter than those belonging to the pyrazolyl substituents in both **12** and **16**.

The electronic spectra of complexes **14**–**17** in solution, measured in $(CH_3)_2SO$, show high energy bands assigned to π–π^* charge-transfer transitions localized on bipyridine ligands in the 294 to 313 nm range. The corresponding absorption bands in the visible region was attributed to MLCT transition bands in analogy to other reported Ru(II) polypyridyl complexes. In particular, the spectra of **14**, **15**, and **17** are similar, displaying a broad band consisting of three absorption bands at 480, 434, and 384 nm for **14**, 483, 438, and 388 nm for **17**, and 466, 418, and 376 nm for **15**, respectively. The visible spectrum of sensitizer **16** displays a broad band at 430 nm. The maximum absorption wavelengths shown by **14**, **15**, and **16** are blue-shifted in the order Cl^-, NCS^-, CN^-, consistent with a decrease of electron density on the metal. In addition, the absorption spectra of **14**, **15**, and **17** display a broad band at approximately 570 nm (530 nm for **15**) expanding in the near-IR region, a characteristic that permits harvesting of less energetic photons. Moreover, the absence of emission by complexes **14**–**17** was attributed to the fact that these complexes are expected to have low-lying triplet ligand field excited states that facilitate rapid non-radiative decay, therefore decreasing the probability of radiative emission.

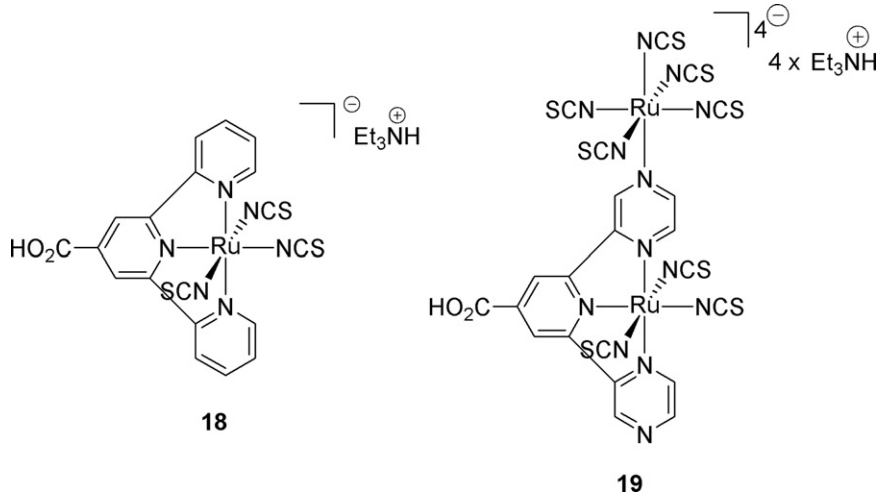

Fig. 12. Terpyridine- and 2,6-dipyrazinylpyridine-coordinated Ru(II) complexes **18** and **19** [167].

The absorption spectra of chemisorbed **14**–**17** on TiO_2 films are broad compared with the corresponding dye peaks in solution, in analogy to sensitizers **12** and **13** (vide supra). Also, the absorption intensity of dye **17**-sensitized TiO_2 films is higher than that of the sensitized films with partially deprotonated **14**, suggesting a more efficient adsorption for **17**. Actually, the amount of adsorbed dye to the surface of the TiO_2 films was determined by desorbing it from the TiO_2 surface into a NaOH aqueous solution. Indeed, the number of adsorbed molecules of the dye adsorbed per square centimeter of geometrical surface area (Γ) is about one order of magnitude higher for **17** than for **14**. The implications of this effect will be extensively discussed in Section 3.2.

More recently, we reported the synthesis, characterization, and TiO_2-sensitizing ability evaluation of Ru(II) dyes **18** and **19**, shown in Fig. 12, which are coordinated with terpyridine and 2,6-dipyrazinylpyridine ligands respectively [167]. Complexes **18** and **19** were characterized by one- and two-dimensional NMR techniques, ESI mass spectrometry, as well as by UV–visible, emission, FTIR, Raman, and cyclic voltammetry studies. Comparison of these two sensitizers with black dye (**1**, Fig. 3) provided more insight into the sensitizers' optimum structure and geometry, paving the way for a more detailed structure-function correlation in these systems.

Complex **18**, isolated in the form of two isomers in a 76/24 molar ratio due to the ambidentate nature of its NCS ligands (N-coordinated NCS versus S-coordinated NCS), was easily prepared via a two-step synthetic route in 57% total isolated yield. The molecular ion of **18** was detected by negative-mode ESI-TOF/MS at $m/z = 552.9160$ (requires 552.9154). Also, the 2,6-dipyrazinylpyridine-substituted analogue of complex **18** was targeted, to study the effect of this more electron-withdrawing ligand on the sensitizing properties of the resulting Ru(II) complex. The preparation of the precursor to the dipyrazinylpyridine analogue of **18** was straightforward; however, in the next step of the synthetic procedure, binuclear complex **19** was isolated instead of the anticipated dipyrazinylpyridine analogue of **18**. NMR data for **19** are consistent with the structure shown in Fig. 12. Moreover, although it had not been possible to observe the molecular tetraanion neither via ESI-TOF/MS nor via ESI/MS, some of the detected fragments could very well originate from complex **19**. For example, the monoanion at $m/z = 772.7612$ in the negative mode ESI-TOF spectrum could be $[M–3NCS]^-$ (requiring 772.7605).

The FTIR spectra of **18** exert pronounced similarities with that of black dye **1** (Fig. 3), as expected. A strong and relatively broad absorption observed at 2104 cm^{-1} was attributed to the characteristic ν(C=N) stretching vibration of both the N- and the S-coordinated NCS ligands (both linkage isomers of complex **18** – vide supra). Also, the two bands at 791 and 764 cm^{-1} [ν(C=S) stretching] were assigned to the all-N- and all-S-coordinated isomers of ruthenium(II) complex **18**, respectively, in close agreement with the corresponding linkage isomers of black dye, where the analogous stretching bands are observed at 788 and 757 cm^{-1}, respectively. Finally, the band at 1693 cm^{-1} was assigned to the C=O stretching band of the protonated carboxyl group in **18**. Dye **19** shows similar characteristics with dyes **1** and **18**, presenting a broad C=N stretching mode at 2098 cm^{-1}, and the C=S modes at 789 and 775 cm^{-1}, due to both N- and S-coordinated NCS ligands. The carboxyl C=O stretching mode in **19** is observed at 1716 cm^{-1}.

Off-resonance Raman peaks of dye **18** under near-IR excitation could not be observed due to the strong photoluminescence band recorded in its emission spectra (vide infra). On the other hand, Resonant Raman spectra of dye **18**, both in the powder form as well as when anchored on the film, are very similar to that of black dye (**1**). The C=N frequency of the NCS ligand is shown at 2120 cm^{-1}, with a shoulder at 2068 cm^{-1}, indicating both N- and S-type coordination to ruthenium(II), in perfect agreement with the IR analysis. Also, it is very interesting that low-frequency modes at 922, 694 (in-plane pyridine deformation), and 535 (out-of-plane pyridine deformation) soften to 890–900, 680, and 530 cm^{-1}, which stems from the missing carboxyl groups on the pyridine moieties of dye **18**. Furthermore, the changes observed in the Resonant Raman spectra of dye **18** upon sensitization of TiO_2 films verify chemisorption of the dye on the semiconducting surface, most likely via bidentate chelation or bridging-type coordination. The analysis of the off-resonance Raman spectra of dye **19** shows several strong lines, due to C=N related vibrations, at 1480 and 1516 cm^{-1}, as well C–N related modes at 1200 and 1282 cm^{-1}, in accordance with results on tris(bipyrazine)ruthenium(II) complexes and heteroleptic complexes with pyridine and bipyrazine. The strong intensity of the above modes is justified by the increased number of such bonds in the pyrazine rings, and the rich spectrum in these regions due to the co-existence of one pyridine moiety. Resonant Raman spectra of dye **19** were obtained by exciting the dye at 514 nm, very close to its MLCT transition (503 nm). Strong modes at 1034 and 1460 cm^{-1}, observed under near-IR excitation, are nearly missing under visible excitation, while, on the other hand, intense modes at 1024 and 1540 cm^{-1} emerge. This is due to the excitation into the MLCT that gives rise to resonance enhancement of symmetric stretching vibrations, and selective enhancement of the pyrazine modes relative to pyridine ones. Finally, Resonant Raman spectra of TiO_2 films sensitized with dye **19** do not show important dif-

ferences as to the corresponding spectra of the dye in the powder form, besides the appearance of the TiO_2 modes. Sharp features, like those observed with dye **18**, were not found in this case suggesting poor dye sensitization of the film.

UV–visible absorption spectra of the dyes were obtained in solution (DMF) as well as upon TiO_2 films, from transmittance and diffuse reflectance experiments respectively. The absorption spectra of dye **18** are dominated by MLCT transitions with absorption maxima at 588, 535 (as a shoulder), and 390 nm. High-energy narrow bands, due to π–π^* intra ligand transitions, are shown at 327 and 280 nm. The molar extinction coefficient at 588 nm is 7640 M^{-1} cm^{-1}. Dye **19**, on the other hand, has a completely different spectrum with a broad MLCT band at 503 nm, and π–π^* transitions at 293 and 265 nm, which are similar to those of tris(bipyrazine)ruthenium(II) complexes. A very broad absorption band at the near-IR region is also observed, possibly due to the $Ru(NCS)_5$ unit. Upon TiO_2 sensitization, the wavelengths of the absorption maxima are only slightly affected. The absorption band of dye **18** keeps its shape, while for dye **19** a clear broadening is observed. This effect could be a sign of possible dye **19** agglomeration on the TiO_2 film. Finally, dye **18** shows an approximate 40 nm blue shift of λ_{max} (0.13 eV or 1060 cm^{-1}) in comparison with black dye (**1**). The emission properties of the dyes were also studied in DMF. From the intersection between the UV–visible and emission spectra of sensitizer **18**, its excitation transition energy was determined to be 1.80 eV (690 nm).

The cyclic voltammogram of dye **18** presents a reversible wave at +0.87 V (versus Ag/AgCl), attributed to the Ru(II)/Ru(III) redox couple, as well as a reversible ligand reduction centered at −1.35 V (versus Ag/AgCl). Using the excitation HOMO–LUMO transition energy value E_{0-0} = 1.80 eV, the LUMO energy level for **18** was estimated to about −0.93 V versus Ag/AgCl. The LUMO levels of both dyes **1** (black dye) and **18** lie well above the TiO_2 conduction band (−0.6 V versus Ag/AgCl) permitting electron injection from the excited dye molecules into the semiconductor conduction band. Greater injection rates are expected for dye **18**, as the driving force (energetic difference between the LUMO of the dye and the conduction band of the semiconductor) is larger than in the case of black dye. The corresponding HOMO levels lie below the I^-/I_3^- redox potential (+0.3 V versus Ag/AgCl) allowing easy cation reduction for both dyes. The CV of binuclear complex **19** was also recorded and presents an irreversible ruthenium(II)-based oxidation wave at +1.35 V (versus Ag/AgCl), together with two quasi irreversible ligand-based reductions centered at −0.66 and −1.14 V (versus Ag/AgCl). The existence of only one oxidation wave in bimetallic complex **19** was attributed to poor electronic communication between the two ruthenium centers and/or low stability of the corresponding oxidized ruthenium species. In the case of complex **19**, the determination of the energetic diagrams was not possible, due to both relative electrochemical irreversibility and poor fitting between the corresponding UV–visible and emission spectra.

The chemisorption of dyes **18** and **19** on the TiO_2 films was quantified to determine the amount of the dye adsorbed. Surface density was estimated to be 2.63×10^{-7} moles cm^{-2} for dye **18**, more than 2.5 times higher than the loading of dye **19** (1.09×10^{-7} moles cm^{-2}). This difference was attributed to the chemical structure of **19** (binuclear), which sterically inhibits its sensitization efficiency by providing much fewer dye monolayers on the TiO_2 semiconductor in comparison with dye **18**. In any case, both complexes present reasonable dye amount values in relation to other efficient dyes, recently reported in literature, implying that light-harvesting efficiency will not be a limiting factor for attaining high photovoltaic efficiency. Moreover, it is interesting to note that both **18** and **19** were adsorbed on TiO_2 to a greater degree than black dye **1**, in qualitative agreement with the reflectance spectra of the dyes on TiO_2 substrates.

4.2. Photoelectrochemical studies

The photoelectrochemical parameters of heteroleptic dyes **12**–**19**, in relation to their active role as providers of photoelectrons in DSSCs, were also determined. Complexes **12** and **13**, bearing the pyrazole-terpyridine based ligand (bdmpp), present similar absorbance in solution as well as when anchored on TiO_2 substrates [162]. This could lead to the conclusion that the two photoelectrodes (i.e. TiO_2 films sensitized by dyes **12** and **13**) possess equivalent dye loading and, thus, their light harvesting efficiency should have been similar. However, this is not reflected in the photocurrent obtained and, consequently, to the measured overall efficiency; Table 3 summarizes the performance parameters obtained by the DSSCs prepared using a liquid electrolyte (Dyesol) and tested under 1 sun AM 1.5 illumination. The DSSCs based on dye **12** produced a continuous short-circuit photocurrent (J_{sc}) as high as 2.97 mA cm^{-2}, an open-circuit photovoltage (V_{oc}) of 573 mV and a fill factor (*FF*) of 0.68, leading to an overall energy conversion efficiency of 1.2%. However, significantly better performance was observed using dye **13**. The corresponding values obtained under similar conditions were: J_{sc} = 8.25 mA cm^{-2}, V_{oc} = 621 mV, *FF* = 0.59 and, finally, an energy conversion efficiency η of 3.0%. The considerable increase of the overall conversion efficiency upon going from **12** to **13** is mainly credited to the about three times rise of the J_{sc} and, to a lesser extent, to the about 50 mV difference in V_{oc} between the two dyes. Still, the above energy conversion efficiency was about the 40% of the efficiency obtained with the prototype

Table 3
Electronic spectroscopic data of dyes bearing tridendate ligands and performance parameters of TiO_2-based DSSCs sensitized by the same dyes.[a]

Ru-photosensitizer	ε[b] (10^4 dm^3 mol^{-1} cm^{-1}) (λ_{max}[c] (nm))	J_{sc}[d] (mA cm^{-2})	V_{oc}[e] (mV)	*FF*[f]	*H*[g] (%)
12	2.0 (450), 2.1 (483)	2.97 (1.38)	573 (491)	0.68 (0.46)	1.2 (0.5)
13	2.2 (432), 2.3 (475)	8.25 (4.29)	621 (584)	0.59 (0.43)	3.0 (1.6)
14	0.7 (434), 0.8 (480)	0.98	493	0.59	0.3
15	0.8 (418), 0.9 (466)	2.07	577	0.65	0.8
16	0.4 (430)	3.14	608	0.66	1.3
17	1.7 (438), 1.7 (483)	3.11	583	0.63	1.1
18	0.8 (588)	0.27	214	0.34	2.5
19	2.3 (503)	6.19	616	0.65	0.02
Black dye	0.9 (627)	10.23	717	0.63	4.6

[a] Parameter values in parentheses correspond to DSSCs prepared using a solidified polymer electrolyte [32]. The cells were illuminated under natural sunlight illumination with a power density of 65.6 mW cm^{-2} (obtained by reference [162]).
[b] Molar absorption coefficient.
[c] Wavelength of maximum absorption.
[d] Short-circuit current.
[e] Open circuit potential.
[f] Fill factor.
[g] Overall power conversion efficiency.

N719 dye (η = 7.3%). Similar results for all dyes (but with decreased values of η) were obtained using a solidified polymer electrolyte replacing the standard liquid redox electrolyte [162]. Taking into account that the only difference between complexes **12** and **13** is the presence of the isothiocyanato ligand (in **13**) instead of a chloride (in **12**), the observed differences in photovoltaic performance can be only ascribed to the significant contribution of the –NCS ligand to the HOMO of the complex, achieving better dye regeneration, due to the direction of the outermost orbitals of the complex towards the electrolyte [168].

Another family of dyes was prepared by utilizing the pyrazole-terpyridine ligand (bpp) shown in Fig. 11. In comparison with bdmpp, bpp has protons instead of methyl groups in the ortho- and para-position of the pyrazole ring. Four different complexes (**14**–**17**) were synthesized, characterized (refer to the previous section) and tested in DSSCs under standard global AM 1.5 illumination conditions: **14** and **15** being [Ru(bpp)(dcbpyH)(X)] (in **14**, X = Cl^- and in **15** X = NCS^-), **16** being the cationic $[Ru(bpp)(dcbpyH_2)Cl]^+$ and **17** being the anionic $[Ru(bpp)(dcbpy)(CN)]^-$. The results are summarized in Table 3, with the most interesting being commented below. At this point, we need to note that probably all four dyes (**14**–**17**) are anchored on the semiconductor surface via one or two (i.e. a bidentate/bridging coordination) carboxyl groups of the unique bipyridine ring and no spectacular differences in performances should be expected from different adsorption mode [121].

Although complexes **14** and **15** differ only in the anionic ligand, their photovoltaic performance was significantly different; solar cells of dye **14** gave a J_{sc} of 0.98 mA cm^{-2}, a V_{oc} of 493 mV and a *FF* of 0.58, yielding an overall power conversion efficiency (η) of 0.3%. Under similar experimental conditions, dye **15** produces higher values of J_{sc} (2.07 mA cm^{-2}), V_{oc} (577 mV) and *FF* (0.65), resulting in an about 3 times higher efficiency (0.8%). Taking into account the fact that dye **14** has a ~3 times larger dye loading and higher absorbance beyond 500 nm [165], the observed differences could be only explained on the basis of the presence of the –NCS ligand, which facilitates dye regeneration, as earlier mentioned in the case of complex **13**. Further efficiency improvement was attained by the addition of one more proton at the carboxylate group of complex **14**, resulting in the anionic complex **16** bearing a fully protonated $dcbpyH_2$ ligand. The latter dye presents similar optical properties with the former one (in solution [165]) but, simultaneously, is more sufficiently adsorbed on the TiO_2 electrodes (about two times higher dye loading was estimated [165]). This effect leads to a J_{sc} enhancement from about 1 up to 3 mA cm^{-2} (by improving the dye loading as well as by releasing protons on its surface and lowering the Fermi-level of TiO_2, thus promoting electron injection [126]) resulting in a conversion efficiency increase from 0.28 to 1.1%, in accordance with analogous reports on carboxylated Ru(II) phenanthroline complexes [169]. Similar efficiencies (or even better ones) attaining values of 1.3% and preserving the high values of J_{sc} were gained using the cationic complex **17** carrying one –CN ligand and no protons (possessing two deprotonated carboxylate groups), despite the lower absorbance and smaller dye loading (in relation to dye **16**). Although this interesting finding is still under investigation, we speculate that either the more electronegative –CN ligand plays the same role as –NCS, promoting dye regeneration, or that the small counterions (Na^+) can more easily access the TiO_2 surface, leading to a downward shift of the conduction band, thereby facilitating electron injection, as De Angelis et al. proposed in a very recent paper [120].

Our results have shown that heteroleptic complexes bearing the bpp or bdmpp ligands do not ensure great photovoltaic performances (not exceeding 1 to 3% conversion efficiency). This is most probably due to difficulties in optimizing the adsorption mode and dipole moment of the dyes [121] a postulate that paved the way to novel homoleptic ruthenium polypyridyl dyes such as **N719** and black dye.

In this context, two novel Ru(II) sensitizers (**18** and **19**) were prepared by mimicking the functionalities of benchmark black dye. In **18**, a terpyridine ligand bearing only one –COOH group in para position was complexed to ruthenium. In another attempt, we targeted at the enhancement of the electron withdrawing nature of the anchoring ligand, substituting terpyridine by monocarboxylated dipyrazinylpyridine; unfortunately, however, a novel, binuclear complex (**19**) was isolated instead (vide supra). In any case, both complexes presented an excellent dye loading when adsorbed TiO_2 photoelectrodes (even better than model black dye that contains two more carboxylic acid moieties [48]), probably due to the great flexibility of the dyes attached via one anchoring group, which would require less space, allowing more dye molecules to adsorb on the titania surface. Thus, we concluded that dye loading would not be a critical parameter for the efficiency of these two novel dyes as sensitizers.

Then, the performance of the DSSCs prepared using the complexes **18** and **19** was thoroughly studied in order to check the molecular structure effects on the overall photovoltaic conversion efficiency. The power conversion efficiency (η) determined for the dye **18**-based cells was as high as 2.5%, with a short-circuit current (J_{sc}) of 6.19 mA cm^{-2}, an open-circuit potential (V_{oc}) of 616 mV, and a filling factor (*FF*) of 0.65 (Table 3). On the other hand, the corresponding efficiency for the dye **19**-based cell was extremely poor (0.02%), obviously due to the molecular structure of the complex. On the other hand, DSSCs prepared using black dye presented an efficiency of 4.6%, about double of that attained by the dye **18** (Table 3), mainly due to the higher photocurrent gained. This result was attributed to a more efficient binding of black dye through the two carboxylic groups (in relation to monocarboxylate bonding in dyes **18** and **19**), allowing for better electron coupling of the dye with the semiconductor (despite the lower dye loading), thereby promoting charge injection from the excited state of the dye [170]. Similar results have been also resolved by other groups studying analogous homoleptic Ru(II) complexes [169,171]. In any case, the obtained efficiency for **18** dye of about 2.5% was very promising.

In order to further improve the above efficiencies, we tried to understand the reasons why the values attained by dye **18** were lower than that attained by the model black dye. The efficiency losses arise mainly from the lower photocurrent (more than 4 mA cm^{-2}), as well as from the lower V_{oc} (about 100 mV). Trying to explain the above differences, the electron dynamics governing the cells constructed with the two different dyes were conducted. Initially, the electron lifetimes were determined by performing Intensity Modulated Voltage Spectroscopy (IMVS) experiments on the two cells (Fig. 13a). It was found that the black dye-based DSSCs clearly present a reduced recombination rate (longer electron lifetimes) [134] than dye **18**-based cell, confirming the differences observed at V_{oc} values (despite the fact that the TiO_2 conduction band is shifted towards more positive potentials upon black dye adsorption).

On the other hand, as noted above, significant differences were observed on the photocurrent delivered by the two cells. The J_{sc} in a DSSC depends on the light harvesting of the photoelectrode, the injection efficiency of the electrons from the dye onto the semiconductor and the collection efficiency of the electrons at the back contact. The light-harvesting of dye **18** is significantly lower than that of black dye above 600 nm; however, this change cannot solely account for the large J_{sc} differences. Differences in charge injection efficiencies (concerning the driving force for electrons injection) are difficult to be evaluated since the LUMO of dye **18** is higher than that of black dye, but, coincidently, the conduction band edge of TiO_2 is also higher upon adsorption of dye **18** in comparison with black dye. Thus, the only possibility that remains to justify the observed

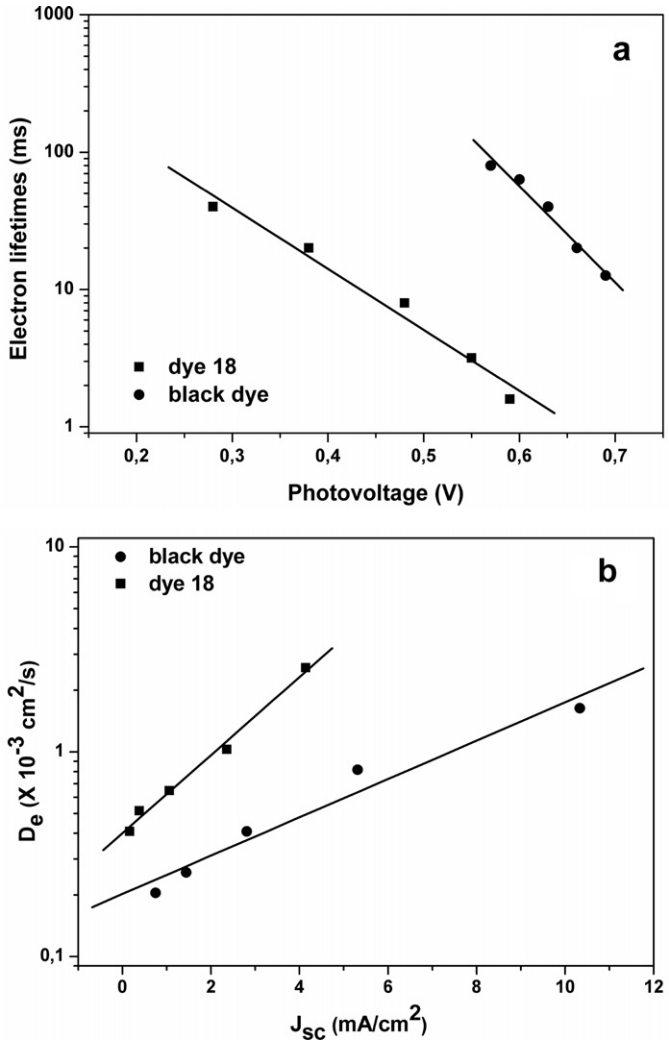

Fig. 13. Electron lifetimes with varying photovoltage (a) electron diffusion coefficients with varying J_{sc} (b) [167].

J_{sc} differences, is the higher charge collection efficiency in the case of black dye. Thus, by estimating the diffusion coefficients at short circuit, by Intensity Modulated Photocurrent Spectroscopy (IMPS) experiments (Fig. 13b), the diffusion lengths (L_n) were determined for the two dyes, being about 45 μm for black dye and only 20 μm for dye **18**. It was then found that black dye had a value of L_n more than double that of dye **18**. We must also highlight the fact that the diffusion length for dye **18** did not overcome the film thickness (being 22 μm), implying that electrons would be lost during their diffusion towards the rear contact. The above observations accurately explained the J_{sc} differences observed between the two dyes. These results are in agreement with other literature reports, which proposed that dyes with a higher number of carboxylic groups (such as black dye in the present case), can affect the dynamics of recombination of the charge-separated state of the dye/TiO_2 moieties in a positive way (in relation to monocarboxylate-containing complexes like dye **18**) [170]. Similar results have been also resolved by other groups studying analogous homoleptic Ru(II) complexes [171].

5. Conclusions

During all these years, our continuous effort in dye synthesis has led to the isolation, characterization and evaluation of a variety of ruthenium(II) complexes bearing different organic ligands. This was achieved by utilizing well established synthetic approaches and by trying bidendate or tridendate pyridyl-based ligands, different counterions and a number of anchoring groups. A key point for the accomplishment of our goals was the continuous and harmonic collaboration between organic, inorganic and theoretical chemists, as well as photoelectrochemists and physicists.

In the field of DSSCs ruthenium dyes' development, and in line with the most recent observations in the literature, our work has led to the conclusion that the existence of as many as possible anchoring groups on the polypyridyl ligands is in favor of efficient sensitization. Additionally, complexes based on tridendate ligands seem to work better than the corresponding dyes bearing bidendate ligands, most probably due to a better stabilization of the ligand in the coordination sphere of the ruthenium metal.

Considering our results and comparing them with very recent literature data, regarding mainly the pivotal dyes **N719** and black dye, we have also concluded that specific requirements are necessary to obtain a highly efficient dye. For example, the specific adsorption mode of homoleptic dyes increases V_{oc}. In addition, there is an optimal degree of protonation for the sensitizer, for which the product of short circuit photocurrent and open circuit potential is the highest possible. Also, tetra butylammonium counterions have proven to cause a modest energy down-shift of the TiO_2 conduction band, due to the fact that they stand far away from the semiconductor surface and, therefore, a maximum V_{oc} is gained (in relation to smaller counterions like Na^+). Finally, to control recombination, the molecular structure of the dye should possess binding sites with a minimum affinity for iodine and the maximum possible distance from the TiO_2 surface.

Acknowledgments

We are most indebted to our co-workers whose names appear in the references for their enthusiasm and their dedicated work. Our work in this research area has been financially supported by the Greek Secretariat for Research and Technology (PENED 03ED 118/2005; 4.5/4.4.1 Competiveness/Infrastructure "EPAN YPODOMON"; EPET II 98AD86; and a Greek-German bilateral collaboration project), NCSR "Demokritos" (Dimoerevna 598 project), the British Council (Greek-British 2004–2006 bilateral collaboration), OrgaPVNet/FP6-Energy-CA (Coordination Action towards stable and low cost organic solar cell technologies and their application), as well as COST CHEMISTRY Actions D14 and D39.

References

[1] Energy and Environment Report 2008, European Environment Agency, Office for Official Publications of the European Communities, Copenhagen, 2008.
[2] N. Armaroli, V. Balzani, Angew. Chem. Int. Ed. 46 (2007) 52.
[3] R.E. Blankenship (Ed.), Molecular Mechanisms of Photosynhtesis, Blackwell Science, Oxford, 2002.
[4] The journal "Inorganic Chemistry" has recently presented a forum on solar and renewable energy: Inorg. Chem. 44 (2005) 6799.
[5] M. Grätzel, Nature 414 (2001) 338.
[6] L.M. Goncalves, V. de Zea Bermudez, H.A. Ribeiro, A.M. Mendes, Energy Environ. Sci. 1 (2008) 655.
[7] This type of cell was reported for the first time in 1991: B. O'Regan, M. Grätzel, Nature 353 (1991) 737s.
[8] The journal "Coordination Chemistry Reviews" has published a special issue on DSSCs: Coord. Chem. Rev. 248 (2004) 1161.
[9] A. Hagfeldt, M. Grätzel, Chem. Rev. 95 (1995) 49.
[10] R. Argazzi, N.Y.M. Iha, H. Zabri, F. Odobel, C.A. Bignozzi, Coord. Chem. Rev. 248 (2004) 1299.
[11] M.K. Nazeeruddin, S.M. Zakeeruddin, J.-J. Lagref, P. Liska, P. Comte, C. Barolo, G. Viscardi, K. Schenk, M. Grätzel, Coord. Chem. Rev. 248 (2004) 1317.
[12] A.S. Polo, M.K. Itokazu, N.Y.M. Iha, Coord. Chem. Rev. 248 (2004) 1343.
[13] G.J. Meyer, Inorg. Chem. 44 (2005) 6852.
[14] N. Robertson, Angew. Chem. Int. Ed. 45 (2006) 2338.
[15] P. Xie, F. Guo, Curr. Org. Chem. 11 (2007) 1272.
[16] T.W. Hamann, R.A. Jensen, A.B.F. Martinson, H. van Ryswyk, J.T. Hupp, Energy Environ. Sci. 1 (2008) 66.
[17] M. Grätzel, Acc. Chem. Res. 42 (2009) 1788.

[18] M.R. Wasielewski, Chem. Rev. 92 (1992) 435.
[19] J.L. Bredas, D. Beljionne, V. Coropceanu, J. Cornil, Chem. Rev. 104 (2004) 4971.
[20] P.J. Cameron, L.M. Peter, J. Phys. Chem. B 109 (2005) 7392.
[21] Q. Wang, S. Ito, M. Grätzel, F. Fabregat-Santiago, I. Mora-Seró, J. Bisquert, T. Bessho, H. Imai, J. Phys. Chem. B 110 (2006) 25210.
[22] Z.-S. Wang, H. Kawauchi, T. Kashima, H. Arakawa, Coord. Chem. Rev. 248 (2004) 1381.
[23] H.-J. Koo, Y.J. Kim, Y.H. Lee, W.I. Lee, K. Kim, N.-G. Park, Adv. Mater. 20 (2008) 195.
[24] B.C. O'Regan, J.R. Durrant, P.M. Sommeling, N.J. Bakker, J. Phys. Chem. C 111 (2007) 14001.
[25] J. Das, F.S. Freitas, I.R. Evans, A.F. Nogueira, D. Khushalani, J. Mater. Chem. 20 (2010) 4425.
[26] A. Kumar, A.R. Madaria, C. Zhou, J. Phys. Chem. C 114 (2010) 7787.
[27] O.K. Varghese, M. Paulose, C.A. Grimes, Nat. Nanotechnol. 4 (2009) 592.
[28] T. Stergiopoulos, A. Ghicov, V. Likodimos, D.S. Tsoukleris, J. Kunze, P. Schmuki, P. Falaras, Nanotechnology 19 (2008) 235602.
[29] L.L. Li, C.Y. Tsai, H.P. Wu, C.C. Chen, E.W.G. Diau, J. Mater. Chem. 20 (2010) 2753.
[30] J. Wang, Z. Lin, Chem. Mater. 22 (2010) 579.
[31] Y. Bai, Y. Cao, J. Zhang, M. Wang, R. Li, P. Wang, S.M. Zakeeruddin, M. Grätzel, Nat. Mater. 7 (2008) 626.
[32] T. Stergiopoulos, I.M. Arabatzis, G. Katsaros, P. Falaras, Nano Lett. 2 (2002) 1259.
[33] L. Wang, S. Fang, Y. Lin, X. Zhou, M. Li, Chem. Commun. (2005) 5687.
[34] H. Nusbaumer, S.M. Zakeeruddin, J.-E. Moser, M. Grätzel, Chem. Eur. J. 9 (2003) 3756.
[35] Z. Zhang, P. Chen, T.N. Murakami, S.M. Zakeeruddin, M. Grätzel, Adv. Funct. Mater. 18 (2008) 341.
[36] M. Wang, N. Chamberland, L. Breau, J.-E. Moser, R. Hymphry-Baker, B. Marsan, S.M. Zakeeruddin, M. Grätzel, Nat. Chem. 2 (2010) 385.
[37] G.R.A. Kumara, A. Konno, K. Shiratsuchi, J. Tsukahara, K. Tennakone, Chem. Mater. 14 (2002) 954.
[38] G. Khelashvili, S. Behrens, C. Weidenthaler, C. Vetter, A. Hinsch, R. Kern, K. Skupien, E. Dinjus, H. Bönnemann, Thin Solid Films 511–512 (2006) 342.
[39] T.N. Murakami, S. Ito, Q. Wang, M.K. Nazeeruddin, T. Bessho, I. Cesar, P. Liska, R. Humphry-Baker, P. Comte, P. Péchy, M. Grätzel, J. Electrochem. Soc. 153 (2006) A2255.
[40] W.K. Lee, E. Ramasamy, D.Y. Lee, J.S. Song, ACS Appl. Mater. Interface 1 (2009) 1145.
[41] W. Hong, Y. Xu, G. Lu, C. Li, G. Shi, Electrochem. Commun. 10 (2008) 1555.
[42] H. Sun, Y. Luo, Y. Zhang, D. Li, Z. Yu, K. Li, Q. Meng, J. Phys. Chem. C 114 (2010) 11673.
[43] M. Wang, A.M. Anghel, B.N.-L. Cevey Ha, N. Pootrakulchote, S.M. Zakeeruddin, M. Grätzel, J. Am. Chem. Soc. 131 (2009) 15976.
[44] K. Hara, T. Sato, R. Katoh, A. Furube, Y. Ohga, A. Shinpo, S. Suga, K. Sayama, H. Sugihara, H. Arakawa, J. Phys. Chem. B 107 (2003) 597.
[45] M.K. Nazeeruddin, A. Kay, I. Rodicio, R. Humphry-Baker, E. Muller, P. Liska, N. Vlachopoulos, M. Grätzel, J. Am. Chem. Soc. 115 (1993) 6382.
[46] M.K. Nazeeruddin, F. De Angelis, S. Fantacci, A. Selloni, G. Viscardi, P. Liska, S. Ito, B. Takeru, M. Grätzel, J. Am. Chem. Soc. 127 (2005) 16835.
[47] M.K. Nazeeruddin, P. Pechy, M. Grätzel, Chem. Commun. (1997) 1705.
[48] M.K. Nazeeruddin, P. Pechy, T. Renouard, S.M. Zakeeruddin, R. Humphry-Baker, P. Comte, P. Liska, L. Cevey, E. Costa, V. Shklover, L. Spiccia, G.B. Deacon, C.A. Bignozzi, M. Grätzel, J. Am. Chem. Soc. 123 (2001) 1613.
[49] Y. Chiba, A. Islam, Y. Watanabe, R. Komiya, N. Koide, L. Han, Jpn. J. Appl. Phys. 45 (2006) L638.
[50] C.Y. Chen, S.J. Wu, C.G. Wu, J.G. Chen, K.C. Ho, Angew. Chem. Int. Ed. 45 (2006) 5822.
[51] C.Y. Chen, S.J. Wu, J.Y. Li, C.G. Wu, J.G. Chen, K.C. Ho, Adv. Mater. 19 (2007) 3888.
[52] M.K. Nazeeruddin, T. Bessho, L. Cevey, S. Ito, C. Klein, F.D. Angelis, S. Fantacci, P. Comte, P. Liska, H. Imai, M. Grätzel, J. Photochem. Photobiol. A: Chem. 185 (2007) 331.
[53] F. Gao, Y. Wang, D. Shi, J. Zhang, M. Wang, X. Jing, R. Humphry-Baker, P. Wang, S.M. Zakeeruddin, M. Grätzel, J. Am. Chem. Soc. 130 (2008) 10720.
[54] F. Gao, Y. Wang, J. Zhang, D. Shi, M. Wang, R. Humphry-Baker, P. Wang, S.M. Zakeeruddin, M. Grätzel, Chem. Commun. (2008) 2635.
[55] F. Matar, T.K. Ghaddar, K. Walley, T. DosSantos, J.R. Durrant, B. O'Regan, J. Mater. Chem. 18 (2008) 4246.
[56] D. Shi, N. Pootrakulchote, R. Li, J. Guo, Y. Wang, S.M. Zakeeruddin, M. Grätzel, P. Wang, J. Phys. Chem. C 112 (2008) 17046.
[57] M. Grätzel, DSC-IC 3, April 23–25, Nara, Japan, 2009.
[58] F. Gao, Y. Cheng, Q. Yu, S. Liu, D. Shi, Y. Li, P. Wang, Inorg. Chem. 48 (2009) 2664.
[59] C.Y. Chen, M. Wang, J.Y. Li, N. Pootrakulcote, L. Alibabaei, C. Ngoc-le, J.D. Decoppet, J.H. Tsai, C. Grätzel, C.G. Wu, S.M. Zakeeruddin, M. Grätzel, ACS Nano 3 (2009) 3103.
[60] J.H. Yum, I. Jung, C. Baik, J. Ko, M.K. Nazeeruddin, M. Grätzel, Energy Environ. Sci. 2 (2009) 100.
[61] T. Bessho, E. Yoneda, J.H. Yum, M. Guglielmi, I. Tavernelli, H. Imai, U. Rothlisberger, M.K. Nazeeruddin, M. Grätzel, J. Am. Chem. Soc. 131 (2009) 5930.
[62] Y. Cao, Y. Bai, Q. Yu, Y. Cheng, S. Liu, D. Shi, F. Gao, P. Wang, J. Phys. Chem. C 113 (2009) 6290.
[63] H.M. Nguyen, R.S. Mane, T. Ganesh, S.H. Han, N. Kim, J. Phys. Chem. C 113 (2009) 9206.
[64] Q. Yu, S. Liu, M. Zhang, N. Cai, Y. Wang, P. Wang, J. Phys. Chem. C 113 (2009) 14559.
[65] M. Wang, S.J. Moon, M. Xu, K. Chittibabu, P. Wang, N. Cevey-Ha, R. Humphry-Baker, S.M. Zakeeruddin, M. Grätzel, Small 6 (2010) 319.
[66] X. Lv, F. Wang, Y. Li, ACS Appl. Mater. Interfaces 2 (2010) 1980.
[67] Y. Sun, A.C. Onicha, M. Myahkostupov, F.N. Castellano, ACS Appl. Mater. Interfaces 2 (2010) 2039.
[68] J.F. Yin, J.G. Chen, Z.Z. Lu, K.C. Ho, H.C. Lin, K.L. Lu, Chem. Mater 22 (2010) 4392.
[69] P. Wang, S.M. Zakeeruddin, J.E. Moser, M.K. Nazeeruddin, T. Sekiguchi, M. Grätzel, Nat. Mater. 2 (2003) 402.
[70] Q. Wang, W.M. Campbell, E.E. Bonfantani, K.W. Jolley, D.L. Officer, P.J. Walsh, K. Gordon, R. Humphry-Baker, M.K. Nazeeruddin, M. Grätzel, J. Phys. Chem. B 109 (2005) 15397.
[71] M. Tanaka, S. Hayashi, S. Eu, T. Umeyama, Y. Matano, H. Imahori, Chem. Commun. (2007) 2069.
[72] L. Giribabu, C.V. Kumar, V.G. Reddy, P.Y. Reddy, C.S. Rao, S.R. Jang, J.H. Yum, M.K. Nazeeruddin, M. Grätzel, Sol. Environ. Mater. Sol. Cell 91 (2007) 1611.
[73] W.M. Campbell, K.W. Jolley, P. Wagner, K. Wagner, P.J. Walsh, K.C. Gordon, L. Schmidt-Mende, M.K. Nazeeruddin, Q. Wang, M. Grätzel, D.L. Officer, J. Phys. Chem. C 111 (2007) 11760.
[74] C.W. Lee, H.P. Lu, C.M. Lan, Y.L. Huang, Y.R. Liang, W.N. Yen, Y.C. Liu, Y.S. Lin, E.W.G. Diau, C.Y. Yeh, Chem. Eur. J. 15 (2009) 1403.
[75] H.P. Lu, C.L. Mai, C.Y. Tsia, S.J. Hsu, C.P. Hsieh, C.L. Chiu, C.Y. Yeh, E.W.G. Diau, Phys. Chem. Chem. Phys. 11 (2009) 10270.
[76] C.P. Hsieh, H.P. Lu, C.L. Chiu, C.W. Lee, S.H. Chuang, C.L. Mai, W.N. Yen, S.J. Hsu, E.W.G. Diau, C.Y. Yeh, J. Mater. Chem. 20 (2010) 1127.
[77] J. He, A. Hagfeldt, S.E. Lindquist, H. Grennberg, F. Korodi, L. Sun, B. Akermark, Langmuir 17 (2001) 2743.
[78] J. He, G. Benko, F. Korodi, T. Polivka, R. Lomoth, B. Akermark, L. Sun, A. Hagfeldt, V. Sundstrom, J. Am. Chem. Soc. 124 (2002) 4922.
[79] E. Palomares, M.V. Martinez-Diaz, S.A. Haque, T. Torres, J.R. Durrant, Chem. Commun. (2004) 2112.
[80] P.Y. Reddy, L. Giribabu, C. Lyness, H.J. Snaith, C. Vijaykumar, M. Chandraskharam, M. Lakshmikantam, J.H. Yum, K. Kalyanasundaram, M. Grätzel, M.K. Nazeeruddin, Angew. Chem. Int. Ed. 46 (2007) 373.
[81] B.E. Hardin, E.T. Hoke, P.B. Armstrong, J.H. Yum, P. Comte, T. Torres, J.M.J. Frechet, M.K. Nazeeruddin, M. Grätzel, M.D. McGehee, Nat. Photon. 3 (2009) 406.
[82] X.F. Wang, C.H. Zhan, T. Maoka, Y. Wada, Y. Koyama, Chem. Phys. Lett. 447 (2007) 79.
[83] X.F. Wang, H. Tamiaki, L. Wang, N. Tamai, O. Kitao, H. Zhou, S.I. Sasaki, Langmuir 26 (2010) 6320.
[84] E. Vrachnou, N. Vlachopoulos, M. Grätzel, J. Chem. Soc. Chem. Commun. (1987) 868.
[85] S. Ferrere, B.A. Gregg, J. Am. Chem. Soc. 120 (1998) 843.
[86] P.M. Jayaweera, S.S. Palayangoda, K. Tennakone, J. Photochem. Photobiol. A: Chem. 140 (2001) 173.
[87] T. Bessho, E.C. Constable, M. Grätzel, A.H. Redondo, C.E. Housecroft, W. Kylberg, M.K. Nazeeruddin, M. Neuburger, S. Schaffner, Chem. Commun. (2008) 3717.
[88] G. Sauve, M.E. Cass, S.J. Doig, I. Lauermann, K. Pomykal, N.S. Lewis, J. Phys. Chem. B 104 (2000) 3488.
[89] S. Altobello, R. Argazzi, S. Caramori, C. Contado, S. Da Fre, P. Rubino, C. Chone, G. Larramona, C.A. Bignozzi, J. Am. Chem. Soc. 127 (2005) 15342.
[90] E.I. Mayo, K. Kilsa, T. Tirrell, P.I. Djurovich, A. Tamayo, M.E. Thompson, N.S. Lewis, H.B. Gray, Photochem. Photobiol. Sci. 5 (2006) 871.
[91] E. Baranhoff, J.-H. Yum, M. Grätzel, M.K. Nazeeruddin, J. Organomet. Chem. 694 (2009) 2661.
[92] A. Islam, H. Sugihara, K. Hara, L.P. Singh, R. Katoh, M. Yanagida, Y. Takahashi, S. Murata, H. Arakawa, Inorg. Chem. 40 (2001) 5371.
[93] E.A.M. Geary, L.J. Yellowlees, L.A. Jack, I.D.H. Oswald, S. Parsons, N. Hirata, J.R. Durrant, N. Robertson, Inorg. Chem. 44 (2005) 242.
[94] For a recent review on organic dyes for DSSCs, see: A. Mishra, M.K.R. Fischer, P. Bauerle, Angew. Chem. Int. Ed. 48 (2009) 2474.
[95] S. Ito, S.M. Zakeeruddin, R. Humphry-Baker, P. Liska, R. Charvet, P. Comte, M.K. Nazeeruddin, P. Pechy, M. Takata, H. Miura, S. Uchida, M. Grätzel, Adv. Mater. 18 (2006) 1202.
[96] S. Hwang, J.H. Lee, C. Park, H. Lee, C. Kim, C. Park, M.H. Lee, W. Lee, J. Park, K. Kim, N.G. Park, C. Kim, Chem. Commun. (2007) 4887.
[97] H. Choi, C. Baik, S.O. Kang, J. Ko, M.S. Kang, M.K. Nazeeruddin, M. Grätzel, Angew. Chem. Int. Ed. 47 (2008) 327.
[98] Z.S. Wang, N. Koumura, Y. Cui, M. Takahashi, H. Sekiguchi, A. Mori, T. Kubo, A. Furube, K. Hara, Chem. Mater. 20 (2008) 3993.
[99] H. Qin, S. Wenger, M. Xu, F. Gao, X. Jing, P. Wang, S.M. Zakeeruddin, M. Grätzel, J. Am. Chem. Soc. 130 (2008) 9202.
[100] S. Ito, H. Miura, S. Uchida, M. Takata, K. Sumioka, P. Liska, P. Comte, P. Pechy, M. Grätzel, Chem. Commun. (2008) 5194.
[101] G. Zhang, H. Bala, Y. Cheng, D. Shi, X. Lv, Q. Yu, P. Wang, Chem. Commun. (2009) 2198.
[102] M. Xu, S. Wenger, H. Bala, D. Shi, R. Li, Y. Zhou, S.M. Zakeeruddin, M. Grätzel, P. Wang, J. Phys. Chem. C 113 (2009) 2966.
[103] H. Im, S. Kim, C. Park, S.H. Jang, C.J. Kim, K. Kim, N.G. Park, C. Kim, Chem. Commun. 46 (2010) 1335.
[104] H. Choi, I. Raabe, D. Kim, F. Teocoli, C. Kim, K. Song, J.H. Yum, J. Ko, M.K. Nazeeruddin, M. Grätzel, Chem. Eur. J. 16 (2010) 1193.

[105] C.H. Chen, Y.C. Hsu, H.H. Chou, K.R.J. Thomas, J.T. Lin, C.P. Hsu, Chem. Eur. J. 16 (2010) 3184.
[106] W. Zeng, Y. Cao, Y. Bai, Y. Wang, Y. Shi, M. Zhang, F. Wang, C. Pan, P. Wang, Chem. Mater. 22 (2010) 1915.
[107] S. Wenger, P.A. Bouit, Q. Chen, J. Teuscher, D. Di Censo, R. Humphry-Baker, J.E. Moser, J.L. Delgado, N. Martin, S.M. Zakeeruddin, M. Grätzel, J. Am. Chem. Soc. 132 (2010) 5164.
[108] S. Ko, H. Choi, M.S. Kang, H. Hwang, H. Ji, J. Kim, J. Ko, Y. Kang, J. Mater. Chem. 20 (2010) 2391.
[109] H. Choi, J.J. Kim, K. Song, J. Ko, M.K. Nazeeruddin, M. Grätzel, J. Mater. Chem. 20 (2010) 3280.
[110] A. Kay, M. Grätzel, J. Phys. Chem. 97 (1993) 6272.
[111] P. Wang, S.M. Zakeeruddin, R. Humphry-Baker, J.E. Moser, M. Grätzel, Adv. Mater. 15 (2003) 2101.
[112] P. Wang, S.M. Zakeeruddin, P. Comte, R. Charvet, R. Humphry-Baker, M. Grätzel, J. Phys. Chem. B 107 (2003) 14336.
[113] K. Hara, Y. Dan-oh, C. Kasada, Y. Ohga, A. Shinpo, S. Suga, K. Sayama, H. Arakawa, Langmuir 20 (2004) 4205.
[114] S. Rühle, M. Greenshtein, S.G. Chen, A. Merson, H. Pizem, C.S. Sukenik, D. Cahen, A. Zaban, J. Phys. Chem. B 109 (2005) 18907.
[115] Z. Zhang, S.M. Zakeeruddin, B.C. O'Regan, R. Humphry-Baker, M. Grätzel, J. Phys. Chem. B 109 (2005) 21818.
[116] N.R. Neale, N. Kopidakis, J. van de Lagemaat, M. Grätzel, A.J. Frank, J. Phys. Chem. B 109 (2005) 23183.
[117] Z. Zhang, N. Evans, S.M. Zakeeruddin, R. Humphry-Baker, M. Grätzel, J. Phys. Chem. C 111 (2007) 398.
[118] K.M. Lee, V. Suryanarayanan, K.C. Ho, K.R. Justin Thomas, J.T. Lin, Sol. Environ. Mater. Sol. Cell 91 (2007) 1426.
[119] J.H. Yum, S.R. Jang, R. Humphry-Baker, M. Grätzel, J.J. Cid, T. Torres, M.K. Nazeeruddin, Langmuir 24 (2008) 5636.
[120] F. De Angelis, S. Fantacci, A. Selloni, M.K. Nazeeruddin, M. Grätzel, J. Phys. Chem. C 114 (2010) 6054.
[121] F. De Angelis, S. Fantacci, A. Selloni, G. Viscardi, M. Grätzel, M.K. Nazeeruddin, Nano Lett. 7 (2007) 3189.
[122] M.K. Nazeeruddin, R. Humphry-Baker, P. Liska, M. Grätzel, J. Phys. Chem. B 107 (2003) 8981.
[123] J. Preat, D. Jacquemin, E.A. Perpète, Energy Environ. Sci. 3 (2010) 891.
[124] S.G. Yan, J.T. Hupp, J. Phys. Chem. 100 (1996) 6867.
[125] W.R. Duncan, C.F. Craig, O.V. Prezhdo, J. Am. Chem. Soc. 129 (2007) 8528.
[126] F. De Angelis, S. Fantacci, A. Selloni, M.K. Nazeeruddin, M. Grätzel, J. Am. Chem. Soc. 129 (2007) 14156.
[127] S. Pelet, J.E. Moser, M. Grätzel, J. Phys. Chem. B 104 (2000) 1791.
[128] B. O'Regan, J. Moser, M. Anderson, M. Grätzel, J. Phys. Chem. 94 (1990) 8720.
[129] A. Zaban, S. Ferrere, B.A. Gregg, J. Phys. Chem. B 102 (1998) 452.
[130] A. Zaban, S. Ferrere, J. Sprague, B.A. Gregg, J. Phys. Chem. B 101 (1997) 55.
[131] S. Ardo, Y. Sun, F.N. Castellano, G.J. Meyer, J. Phys. Chem. B 114 (2010) 14596.
[132] U.B. Cappel, S.M. Feldt, J. Schöneboom, A. Hagfeldt, G. Boschloo, J. Am. Chem. Soc. 132 (2010) 9097.
[133] B. O'Regan, I. López-Duarte, M.V. Martinez-Diaz, A. Forneli, J. Albero, A. Morandiera, E. Palomares, T. Torres, J.R. Durrant, J. Am. Chem. Soc. 130 (2008) 2907.
[134] J.N. Clifford, E. Palomares, M.K. Nazeeruddin, M. Grätzel, J. Nelson, X. Li, N.J. Long, J.R. Durrant, J. Am. Chem. Soc. 126 (2004) 5225.
[135] A. Reynal, A. Forneli, E. Martinez-Ferrero, A. Sánchez-Díaz, A. Vidal-Ferran, B.C. O'Regan, E. Palomares, J. Am. Chem. Soc. 130 (2008) 13558.
[136] B. O'Regan, K. Walley, M. Juozapavicius, A. Anderson, F. Matar, T. Ghaddar, S.M. Zakeeruddin, C. Klein, M. Grätzel, J. Am. Chem. Soc. 131 (2009) 3541.
[137] B.C. O'Regan, J.R. Durrant, Acc. Chem. Res. 42 (2009) 1799.
[138] V. Likodimos, T. Stergiopoulos, P. Falaras, R. Harikisun, J. Desilvestro, G. Tulloch, J. Phys. Chem. C 113 (2009) 9412.
[139] T. Stergiopoulos, M.-C. Bernard, A. Hugot-Le Goff, P. Falaras, Coord. Chem. Rev. 248 (2004) 1407.
[140] M.-C. Bernard, H. Cachet, P. Falaras, A. Hugot-Le Goff, M. Kalbac, I. Lukes, N.T. Oanh, T. Stergiopoulos, I. Arabatzis, J. Electrochem. Soc. 150 (2003) E155.
[141] A.G. Kontos, T. Stergiopoulos, G. Tsiminis, Y.S. Raptis, P. Falaras, Inorg. Chim. Acta 361 (2008) 761.
[142] K.-L. Wu, H.-C. Hsu, K. Chen, Y. Chi, M.-W. Chung, W.-H. Liu, P.-T. Chou, Chem. Commun. 46 (2010) 5124.
[143] D. Kuang, C. Klein, H.J. Snaith, J.-E. Moser, R. Humphry-Baker, P. Comte, S.M. Zakeeruddin, M. Grätzel, Nano Lett. 6 (2006) 769.
[144] D.R. Jones, A. Troisi, Phys. Chem. Chem. Phys. 12 (2010) 4625.
[145] Y.M. Rhee, M. Head-Gordon, J. Phys. Chem. A 111 (2007) 5314.
[146] M. Pastore, E. Mosconi, F. De Angelis, M. Grätzel, J. Phys. Chem. C 114 (2010) 7205.
[147] G. Konti, E. Chatzivasiloglou, V. Likodimos, G. Kantonis, A.G. Kontos, A.I. Philippopoulos, P. Falaras, Photochem. Photobiol. Sci. 8 (2009) 726.
[148] P.A. Lay, A.M. Sargeson, H. Taube, Inorg. Synth. 24 (1986) 291.
[149] J.G.C. Veinot, A.A. Farah, J. Galloro, F. Zobi, V. Bell, W.J. Pietro, Polyhedron 19 (2000) 331.
[150] A.A. Farah, J.G.C. Veinot, M. Najman, W.J. Pietro, Pure Appl. Chem. A37 (2000) 1507.
[151] P. Pearson, A.M. Bond, G.B. Deacon, C. Forsyth, L. Spiccia, Inorg. Chim. Acta 361 (2008) 601.
[152] S. Anderson, E.C. Constable, K.R. Seddon, J.E. Turp, J.E. Baggot, M.J. Pilling, Dalton Trans. (1985) 2247.
[153] R. Caspar, H. Amouri, M. Gruselle, C. Cordier, B. Malézieux, R. Duval, H. Leveque, Eur. J. Inorg. Chem. (2003) 499.
[154] C. Klein, M.K. Nazeeruddin, D. Di Censo, P. Liska, M. Grätzel, Inorg. Chem. 43 (2004) 4216.
[155] P.W. Hansen, P.E.W. Jensen, Spectrochim. Acta 50A (1994) 169.
[156] A. Juris, V. Balzani, F. Barigelletti, S. Campagna, P. Belser, A. von Zelewsky, Coord. Chem. Rev. 84 (1988) 85.
[157] M.K. Nazeeruddin, S.M. Zakeeruddin, R. Humphry-Baker, M. Jirousek, P. Liska, N. Vlachopoulos, V. Shklover, C.-H. Fischer, M. Grätzel, Inorg. Chem. 38 (1999) 6298.
[158] C. Bauer, G. Boschloo, E. Mukhtar, A. Hagfeldt, J. Phys. Chem. B 106 (2002) 12693.
[159] E. Chatzivasiloglou, O. Igglessi-Markopoulou, V. Likodimos, G. Konti, G. Kantonis, A.I. Philippopoulos, P. Falaras, unpublished results.
[160] K. Kalyanasundaram, M. Grätzel, J. Coord. Chem. Rev. 77 (1998) 347.
[161] K. Hara, H. Horiuchi, R. Katoh, L.P. Singh, H. Sugihara, K. Sayama, S. Murata, M. Tachiya, H. Arakawa, J. Phys. Chem. B 106 (2002) 374.
[162] T. Stergiopoulos, S. Karakostas, P. Falaras, J. Photochem. Photobiol. A: Chem. 163 (2004) 331.
[163] K. Chryssou, V.J. Catalano, R. Kurtaran, P. Falaras, Inorg. Chim. Acta 328 (2002) 204.
[164] K. Chryssou, T. Stergiopoulos, P. Falaras, Polyhedron 21 (2002) 2773.
[165] A.I. Philippopoulos, A. Terzis, C.P. Raptopoulou, V.J. Catalano, P. Falaras, Eur. J. Inorg. Chem. (2007) 5633.
[166] C.A. Bessel, R.F. See, D.L. Jameson, M.R. Churchill, K.J. Takeuchi, J. Chem. Soc., Dalton Trans. (1993) 1563.
[167] G.C. Vougioukalakis, T. Stergiopoulos, G. Kantonis, A.G. Kontos, K. Papadopoulos, A. Stublla, P.G. Potvin, P. Falaras, J. Photochem. Photobiol. A: Chem. 214 (2010) 22.
[168] A. Hagfeldt, M. Grätzel, Acc. Chem. Res. 33 (2000) 269.
[169] K. Hara, H. Sugihara, L.P. Singh, A. Islam, R. Katoh, M. Yanagida, K. Sayama, S. Murata, H. Arakawa, J. Photochem. Photobiol. A: Chem. 145 (2001) 117.
[170] A. Fillinger, B.A. Parkinson, J. Electrochem. Soc. 146 (1999) 4559.
[171] K. Kilså, E.I. Mayo, B.S. Brunschwig, H.B. Gray, N.S. Lewis, J.R. Winkler, J. Phys. Chem. B 108 (2004) 15640.